HHS Public Access

Author manuscript

Nat Immunol. Author manuscript; available in PMC 2024 May 01.

Published in final edited form as:

Nat Immunol. 2023 November ; 24(11): 1879–1889. doi:10.1038/s41590-023-01637-4.

Fungal microbiota sustains lasting immune activation of neutrophils and their progenitors in severe COVID-19

Takato Kusakabe[1,2], **Woan-Yu Lin**[1,2,13], **Jin-Gyu Cheong**[6,13], **Gagandeep Singh**[7,8], **Arjun Ravishankar**[6], **Stephen T. Yeung**[1,11], **Marissa Mesko**[1,2], **Meghan Bialt DeCelie**[1,2], **Guilhermina Carriche**[1,2], **Zhen Zhao**[6], **Sophie Rand**[6], **Itai Doron**[1,2], **Gregory G. Putzel**[2], **Stefan Worgall**[5,13], **Melissa Cushing**[6], **Lars Westblade**[6], **Giorgio Inghirami**[6], **Christopher N. Parkhurst**[1,2], **Chun-Jun Guo**[1,2,13], **Michael Schotsaert**[7,8], **Adolfo García-Sastre**[7,8,9,10], **Steven Z. Josefowicz**[6,13], **Mirella Salvatore**[3,4], **Iliyan D. Iliev**[1,2,12,13,*]

[1]Joan and Sanford I. Weill Department of Medicine, Weill Cornell Medicine, New York, NY 10021, USA.

[2]The Jill Roberts Institute for Research in Inflammatory Bowel Disease, Weill Cornell Medicine, New York, NY 10021, USA.

[3]Public Health Programs Division, Joan and Sanford I. Weill Department of Medicine, Weill Cornell Medicine, New York, NY 10065, USA.

[4]Department of Population Health Sciences, Weill Cornell Medicine, New York, NY 10065, USA.

[5]Department of Pediatrics, Weill Cornell Medicine, New York, NY 10065, USA.

[6]Department of Pathology and Laboratory Medicine, Weill Cornell Medicine, New York, NY 10065, USA.

[7]Department of Microbiology, Icahn School of Medicine at Mount Sinai New York, NY, 10029, USA.

[8]Department of Medicine, Division of Infectious Diseases, Icahn School of Medicine at Mount Sinai New York, NY, USA

[*]Corresponding senior author: iliev@med.cornell.edu.

Author contribution

TK and IDI conceived and conceptualized the study. TK, GS, JC, AR, STY, M Schotsaert designed experiments and analyzed data, M Salvatore was involved in investigation, clinical samples and clinical data acquisition, TK, WYL, JC, GS, GC, STY, CJG, MM, MBD, ID and GGP performed experiments, acquired and analyzed data. SR, MC, LW, CNP, ZZ and GI provided clinical samples and participated in clinical data acquisition. SW, LN contributed to experimental interpretation. IDI, M Salvatore, AGS and SZJ supervised the study. TK, JC, WYL and IDI generated figures and legends from analyzed data. IDI administered the project and acquired funding. TK and IDI wrote the manuscript.

Declaration of Interests

The AGS laboratory has received research support from GSK, Pfizer, Senhwa Biosciences, Kenall Manufacturing, Blade Therapeutics, Avimex, Johnson & Johnson, Dynavax, 7Hills Pharma, Pharmamar, ImmunityBio, Accurius, Nanocomposix, Hexamer, N-fold LLC, Model Medicines, Atea Pharma, Applied Biological Laboratories and Merck, outside of the reported work. A.G.-S. has consulting agreements for the following companies involving cash and/or stock: Castlevax, Amovir, Vivaldi Biosciences, Contrafect, 7Hills Pharma, Avimex, Pagoda, Accurius, Esperovax, Farmak, Applied Biological Laboratories, Pharmamar, CureLab Oncology, CureLab Veterinary, Synairgen, Paratus, Pfizer and Prosetta, outside of the reported work. A.G.-S. has been an invited speaker in meeting events organized by Seqirus, Janssen, Abbott and Astrazeneca. A.G.-S. is inventor on patents and patent applications on the use of antivirals and vaccines for the treatment and prevention of virus infections and cancer, owned by the Icahn School of Medicine at Mount Sinai, New York, outside of the reported work. M Schotsaert has received unrelated research funding in sponsored research agreements from ArgenX BV, Moderna, 7Hills Pharma and Phio Pharmaceuticals which has no competing interest with this work. The other authors declare no competing interests related to this study.

[9]Department of Pathology, Molecular and Cell-Based Medicine, Icahn School of Medicine at Mount Sinai New York, NY, USA

[10]Global Health and Emergent Pathogens Institute and the Tisch Cancer Institute, Icahn School of Medicine at Mount Sinai, New York, NY, 10029, USA.

[11]Department of Microbiology, New York University, Langone Health, New York, NY, 10016, USA

[12]Department of Microbiology and Immunology, Weill Cornell Medicine, New York, NY 10065, USA.

[13]Immunology and Microbial Pathogenesis Program, Weill Cornell Graduate School of Medical Sciences, Weill Cornell Medicine, Cornell University, New York, NY 10065, USA.

Abstract

Gastrointestinal fungal dysbiosis is a hallmark of several diseases marked by systemic immune activation. Whether persistent pathobiont colonization during immune alterations and impaired gut barrier function has a durable impact on host immunity is unknown. We found that elevated levels of *C. albicans* IgG antibodies marked severe COVID-19 patients (sCOVID-19) who suffered intestinal *Candida* overgrowth, mycobiota dysbiosis and systemic neutrophilia. Analysis of hematopoietic stem cell progenitors in sCOVID-19 revealed transcriptional changes in antifungal immunity pathways and reprogramming of granulocyte myeloid progenitors (GMPs) for up to a year. Mice colonized with *C. albicans* patient isolates experienced increased lung neutrophilia and pulmonary NETosis during SARS-CoV-2 infection, which were partially resolved with antifungal treatment or by IL-6R blockade. sCOVID-19 patients treated with tocilizumab experienced sustained reductions in *C. albicans* IgG antibodies titers and GMP transcriptional changes. These findings suggest that gut fungal pathobionts may contribute to immune activation during inflammatory diseases, offering potential mycobiota-immune therapeutic strategies for sCOVID-19 with prolonged symptoms.

Keywords

Mycobiome; COVID-19; neutrophils; IL-6; Neutrophil extracellular traps (NETs); tocilizumab; granulocyte monocyte progenitors (GMP); hematopoietic stem and progenitor cells (HSPC); antifungal IgG antibodies; SARS-CoV-2

Severe acute respiratory syndrome coronavirus-2 (SARS-CoV-2), the causative agent of COVID-19, has infected more than 700 million people worldwide, causing over 7 million deaths to date[1]. In addition to all described sympthoms[2], millions of individuals who have recovered from acute COVID-19 infection suffer post-acute sequelae of COVID-19 (PASC) or long-COVID, manifesting with memory loss, fatigue and gastrointestinal (GI) distress[3]. Although mechanisms leading to disease exacerbation are still under investigation, immune dysregulation is a key characteristic of COVID-19 pathophysiology[4].

Studies have reported substantial involvement of the gastrointestinal tract in the pathophysiology of several inflammatory diseases, including severe COVID-19 (sCOVID-19)[5-7]. COVID-19 patients present with altered gut microbial composition and

gut barrier dysfunction, which could increase the translocation of bacterial products and toxins into the circulation and exacerbate the inflammatory response systemically and at distal sites[8,9]. Beyond bacteria, the fungal microbiota (mycobiota) can activate protective or proinflammatory immunity in a context-dependent manner[10]. Fungi are common inhabitants of the human gastrointestinal tract and can contribute to intestinal, airways and systemic inflammation during pathophysiological conditions[11,12]. Dangerous secondary lung infections with *Aspergillus spp.* and *Mucor spp.* have been reported in critically ill COVID-19 patients[13] and changes in intestinal mycobiota composition have been observed in sCOVID-19 patients [14,15]. Despite these correlations, it is currently unknown whether persistent alterations of intestinal mycobiota in conditions of impaired gut barrier function and prolonged immune activation has an impact on host immunity in sCOVID-19.

Here, we demonstrate the contribution of intestinal fungal pathobiont to the immunopathology of sCOVID-19 through the activation of neutrophils and their progenitors. This effect is IL-6-dependent and persists for up to a year after recovery, as indicated by elevated anti-*Candida* antibodies and activation of antifungal immune pathways in GMPs. Experiments with *C. albicans* in mice revealed increased lung neutrophilia and pulmonary NETosis during SARS-CoV-2 infection, which was partially alleviated with antifungal treatment or IL-6R blockade. These findings underscore the lasting impact of intestinal fungal pathobionts on host immunity and pulmonary inflammation in situations involving ongoing immune alterations and impaired gut barrier function, as seen in sCOVID-19.

RESULTS

sCOVID-19 develop antibodies to intestinal fungi

The induction of systemic antifungal IgG antibodies has been an important readout for immune responses to fungal microbiota during homeostasis or in several immune-mediated diseases[16]. Because antibodies against fungal mannan (*Saccharomyces cerevisiae* antibodies, ASCA) are increased in patients with immune-mediated pathologies targeting the gastrointestinal tract, such as Crohn's Disease (CD)[17], we characterized ASCA responses in a cohort (hereafter cohort 1) of COVID-19 patients treated at Weill Cornell Medicine / NewYork-Presbyterian Hospital in March-July 2020, during the first wave of SARS-CoV-2 infections (Supplementary Table 1). We recruited 91 COVID-19 patients, 25 of whom had moderate/mild disease (hereafter mCOVID-19), defined as SARS-CoV-2 infection and <6 liters/min noninvasive supplemental oxygen to maintain SpO2 >92%, and 66 with severe disease, defined as requiring oxygen at a flow rate higher than 6 litters/min or by an advanced oxygen delivery device including invasive mechanical ventilation. 36 individuals that were never exposed to the virus and tested negative for antibodies to SARS-CoV-2 Spike protein were used as healthy individuals (HD; Extended Data Fig. 1a-c). Serological analysis indicated a significant increase of ASCA IgG in COVID-19 patients when compared to HD (Fig. 1a), despite no reports of clinical or laboratory evidence of overt fungal superficial or systemic infection in this cohort. The overall increase was comparable to ASCA titers in a cohort of CD patients (Fig. 1a), suggesting that, similar to patients that suffer from a chronic intestinal disease[12,18], COVID-19 patients developed antibodies to fungi. In CD, ASCA may arise in response to fungal species due to the common presence of

mannan in fungal cell walls[16]. To identify fungal antibody targets in COVID-19 patients, we assessed the systemic IgG specificities against fungal species commonly associated with the human gut, oral and skin mucosa, as well as environmental fungal species that can lead to serious lung infections in humans[19]. Because COVID-19 clinical manifestations and fungal immune recognition are characterized by specific cellular, cytokine and humoral profiles[9,20], we also assessed whether fungal antibody profiles associated with disease severity. This analysis indicated considerable increases of IgG antibody titers to *C. albicans* (ACAL IgG, 3.70 fold), *C. parapsilosis* (3.96 fold) and *S. cerevisiae* (4.18 fold) in the plasma of sCOVID-19 when compared to HD (Fig. 1b). In contrast, IgG antibodies against fungi that can affect the lung[21] or reside on the skin, such as *Aspergillus, Alternaria* and *Malassezia* species, remained unchanged (Fig. 1c). ICU admission by itself can lead to increased fungal exposure[22]. In 5 patients admitted to the intensive care unit for diseases not related to COVID-19 (nonCOV, cohort 2) we did not observe increased ACAL IgG compared to sCOVID-19 (Supplementary Table 2 and Fig. 1d), suggesting that the increase in ACAL and ASCA titers was not a consequence of ICU admission. This data suggested that antifungal antibodies in COVID-19 patients were elicited by a specific subset of the gut mycobiota.

To assess whether the high titers of antifungal antibodies were present before SARS-CoV-2 infection or were generated during disease we assessed samples from a longitudinal sampling (thereafter cohort 2) collected at clinical diagnosis of infection (V1) and during acute disease (more than 2 weeks after the initial diagnosis, V2) in mCOVID-19 patients (n=6) and sCOVID-19 (n=6). We found no increase of antifungal antibody titers at V2 in mCOVID-19 compared to those at V1 (Fig. 1e). In contrast, a significant increase of ACAL and ASCA titers was detected at V2 in sCOVID-19 (Fig. 1e). These results indicate that an antibody response to specific fungi developed in sCOVID-19 while such increased antibody titers were not detected before infection.

Gut *Candida* expansion correlates with COVID-19 severity

Gut mycobiota composition has been extensively studied in multiple human cohorts[23] and internal transcribed spacer (ITS) sequencing analyses have reported gut fungal dysbiosis in a cohort of COVID-19 patients[14,15]. To address whether SARS-COV-2 infection impact on gut mycobiota, we performed an ITS-1-based barcoding approach to deep sequence the ITS-1 regions of fungal rDNA from fecal samples collected at the time of hospitalization from 10 COVID-19 patients (cohort 3), of which 3 had sCOVID-19 and 7 mCOVID-19, as well as from 10 HD (Supplementary Table 3). We found that patients with COVID-19 had an increased fungal load in fecal samples compared with uninfected control, and that the gut mycobiota was dominated by the Basidiomycota and Ascomycota phyla (Extended Data Fig. 2a), similar to the phyla composition in multiple human cohorts[18,23]. Mycobiota taxonomic composition indicated that *Candida* and *Saccharomyces spp.* were the most common fungal genera detected in both COVID-19 and HD groups (Fig. 2a). Fungal diversity decreased in COVID-19 samples compared to HD, consistent with fungal dysbiosis in COVID-19 patients[15]. Compared to HD controls, patients with COVID-19 showed an increased relative abundance of fecal *Candida* spp., while the relative abundance of other fungal genera was similar between the two groups (Fig. 2b and Extended Data Fig. 2b). The relative expansion of *Candida* spp. correlated with a decreased relative abundance of anaerobic

bacterial genera such as *Clostridiales* and *Lachnospiraceae* (Fig. 2c, d), consistent with other studies exploring transkingdom relations between fungi and bacteria[24].

To evaluate whether changes in the relative abundance of *Candida* spp. are due to fungal expansion, we assessed the fungal biomass using a multiKAP approach[25], which can distinguish fungal from bacterial cells by staining with the fungal cell wall binding dye calcofluor white (CFW). Expansion of the fungal biomass was more prevalent in the gut of COVID-19 patients compared to HD (Fig. 2e). Based on the results of the ITS sequencing, we developed a culture-based approach to isolate, identify and collect live fungi from fecal samples of mCOVID-19 and sCOVID-19. *C. albicans* was common in the gut of COVID-19 patients and expanded in the culture from fecal samples of COVID-19 patients independent of antibiotic therapy (Supplementary Table 4). Notably, *Candida* growth (CFU/g feces) correlated with disease severity (Fig. 2f), suggesting an association between intestinal overgrowth of *C. albicans* strains and severe COVID-19.

Gut fungal dysbiosis was reported to aggravate disease severity in airway inflammation[11,26]. To test whether specific fungal species in the gut mycobiota play a role in COVID-19 by priming aberrant immunity, we colonized C57BL/6J mice with *Candida* strains isolated from the gut of COVID-19 patients (hereafter referred to as COVCa). Mice colonized with COVCa for two weeks had a significant increase of circulating ACAL antibodies in the blood, while mice colonized with *C. glabrata* isolated from a COVID-19 patient (COVCg) did not, compared with non-colonized mice (Fig. 2g, Extended Data Fig. 3a). This finding was confirmed using multiple *C. albicans* (COVCa1,COVCa2 and COVCa5) isolates (Extended Data Fig. 3b). The magnitude of antibody titers induction was dependent on the COVCa strain; titers increased 45.5, 342.6 and 41.6 fold in COVCa1, COVCa2 and COVCa5-colonized mice, respectively, compared to non-colonized mice (Extended Data Fig. 3b), as previously reported for gut T_H17 cell responses in the context of IBD[27], suggesting that the intestinal expansion of *C. albicans* could be responsible for the observed increase of fungal IgG antibodies in the serum of COVID-19 patients and that ACAL IgG antibodies might serve as a surrogate marker of the host response to intestinal *C. albicans*.

Systemic neutrophilia in sCOVD-19 associate with ACAL IgG levels

Neutrophils have a key role in the development of severe COVID-19[28]. Increased serum levels of neutrophil-released calprotectin, which associates with the severity of the pathogen-associated tissue damage or with excessive cytokine storm, has been reported in patients with severe COVID-19[28]. We found increased calprotectin in the plasma of sCOVID-19 compared to HD (Fig. 3a). To assess the general landscape of immune response during COVID-19, we performed extensive immunophenotyping to characterize the frequency of circulating immune subsets in 30 patients (17 mCOVID-19 and 13 sCOVID-19) from cohort 1 (Supplementary Table 1)[29]. Flow-cytometry based immune cell profiling of peripheral blood showed a strong correlation between the presence of ACAL IgG and frequency of $Lin^{-}CD11b^{+}CD33^{+}$ myeloid cell in sCOVID-19, but not in mCOVID-19 (Fig. 3b, linear regression with interaction term, p=0.005). There was no correlation between ACAL IgG and the lymphoid compartment (Fig. 3b, interaction p=0.117) or specific populations of lymphocytes such as $CD3^{-}CD56^{+}CD16^{+}$NK cells,

$CD3^+CD4^+$ T cells, $CD3^+CD8^+$ T cells and $CD19^+B220^+$ B cells (Extended Data Fig. 4a-e). We observed a global loss of lymphocytes among $CD45^+$ cells and an enrichment of the myeloid cell compartment in the peripheral blood of sCOVID-19 compared to mCOVID-19 or HD (Fig. 3c), consistent with other reports[30]. Deeper analysis showed that a population of $Lin^-CD11b^+CD16^+CD14^-CD15^+$ polymorphonuclear neutrophils/granulocytes (PMNs), but not $Lin^-CD11b^+CD16^+CD14^+CD15^+$ monocytes (MO) and $Lin^-CD11b^+CD16^+CD14^-CD15^+$ monocyte-derived cells (MC), was responsible for this signal (Fig. 3c). These findings were corroborated by positive correlation between ACAL IgG and plasma calprotectin levels in peripheral blood (Fig. 3d). Neutrophils can be induced by intestinal colonization with laboratory strain of *C. albicans*[31]. Immune cell profiling of peripheral blood and lungs from COVCa5-, COVCg3- or non-colonized mice (Extended Data Fig. 3c) showed that intestinal colonization with COVCa5, but not with COVCg3, led to an increased frequency and absolute numbers of circulating $Ly\text{-}6G^+CD11b^+$ neutrophils in the blood and the lungs of mice two weeks after colonization compared to those of non- and COVCg3- colonized mice (Extended Data Fig. 3c,d). Notably, treatment with the antifungal drug fluconazole dampened the number of $Ly\text{-}6G^+CD11b^+$neutrophils in the blood and lung of COVCa5-colonized mice and reduced the expression of calprotectin in the serum compared to non-colonized mice (Fig. 3e,f). This data suggested that the increase in intestinal *C. albicans* correlated with the frequency of polymononuclear neutrophils and the level of the inflammatory marker calprotectin in severe COVID-19.

Altered GMPs function persists after sCOVD-19 recovery

Many patients who have recovered from acute COVID-19 infection experience persistent or new symptoms for four weeks or more following the initial SARS-CoV-2 infection[32], which lead to significant disability and impairment of normal daily life. This post-acute sequela of SARS CoV-2 infection (PASC) is suspected to be in part related to aberrant cellular or humoral immune responses to self- and microbiota-derived antigens. To identify mycobiota-related immune features in COVID-19 patients, we collected convalescent plasma and PBMC samples at month 2-4 post-disease onset (early recovery) or month 4-12 (late recovery) from patients in cohort 2 (Supplementary Table 2), who were monitored in ICU for 2-4 months as intermediate care until discharged, and then seen as out-patients in post-ICU clinic for 4-12 months. In cohort 3, we assessed plasma antibody titer against fungi and expression of calprotectin in mCOVID-19 (early recovery, n=7, late recovery, n=5), sCOVID-19 (early recovery, n=10, late recovery, n=14) and HD (n=8). Higher levels of ACAL antibodies were detected in convalescent patients who had experienced severe disease compared to those with mCOVID-19 or HD at early recovery, and high ACAL levels persisted for up to 12 months (last time point we measured; Fig. 4a). On the other hand, the titers of antibodies against *A. fumigatus* and bacterial flagellin were similar across all groups (Fig. 4a). This data suggested a lasting antifungal antibody signature in patients recovering from sCOVID-19.

Increased numbers of circulating neutrophils with an inflammatory phenotype have been reported in sCOVID-19 patients with persistent pulmonary symptoms 3 to 6 months post-disease onset[33]. Calprotectin levels, which were assessed as a proxy of the frequency of circulating neutrophils, were elevated at month 2-4 post-disease onset, but significantly

declined at month 4-12 in sCOVID-19 patients (Fig. 4b), suggesting that neutrophils returned to pre-sCOVID-19 levels during late recovery. Altered immune cell composition, neutrophil function and hematopoiesis that persists months after infection has been reported in sCOVID-19 patients[33,34]. To determine whether sCOVID-19 induced changes in the hematopoietic stem and progenitor cells (HSPC) compartment that were retained during convalescence, we enriched $CD34^+$HSPC from the peripheral blood mononuclear cells (PBMC) of HD (n=5), sCOVID-19 (n=12) and nonCOV (n=5) (cohort 2) and performed scRNA-seq. We acquired 28,069 peripheral $CD34^+$ HSPC and identify differentially expressed genes among the 10 resulting subclusters[34] after pre-processing and cell-type annotation (Fig. 4c). HSPC subsets were manually annotated as hematopoietic stem cells and multipotent progenitors (HSC/MPP), lymphoid-primed MPP (LMPP), megakaryocyte erythroid progenitors (MEP), erythroid progenitors (Ery), granulocyte monocyte progenitors (GMP) and basophil-eosinophil-mast cell progenitors (BEM) based on the marker gene expression[34] (Fig. 4c). We detected increased transcription of genes encoding C-type lectin receptors (*CLEC7A, CLEC6A, CLEC4E*), downstream signaling molecules (*MALT1, SYK, BAK1, BTK*) and Toll-like receptor 2 in $CD34^+$HPSCs from sCOVID-19 compared with HD (Fig. 4d). Increased frequency of GMPs was observed in early and late recovery sCOVID-19 (Fig. 4e), and positively associated with ACAL IgG titers from convalescent plasma (Fig. 4f and Extended Data Fig. 5). Furthermore, GMP from sCOVID-19 had high expression of *MPO* and *ELANE* genes, which encode for neutrophil granule proteins myeloperoxidase (MPO) and elastases, compared to HD (Fig. 4g). Together, these observations suggested that gut commensal fungal opportunists such as *C. albicans* might contribute to long-lasting alterations in neutrophil progenitors associated with prolonged COVID-19.

C. albicans affects ACAL and GMP activation through IL-6R and fosters lung NETosis during SARS-CoV-2 infection

Assessment of multiple cytokines in mice intestinally colonized with *C. albicans* showed an increase of IL-6 in the serum[35]. Because gut *C. albicans* can affect systemic immunity[25] and neuronal function through cytokine-mediated mechanisms[35], we tested whether *C. albicans*-induced IL-6R contributed to the induction of neutrophilia. C57BL/6J mice colonized with COVCa5 showed a significant increase in blood circulating Ly-$6G^+CD11b^+$ neutrophils and ACAL antibodies two weeks after colonization, while COVCa5-colonized mice treated intraperitoneally with IL-6R neutralizing antibodies the day before colonization showed a decrease in ACAL antibodies in the serum and a decrease in the frequency of Ly-$6G^+CD11b^+$ neutrophils in peripheral blood and the lung two weeks post-COVCa5 colonization compared to COVCa5-colonized mice without IL-6R neutralizing antibodies (Fig. 5a-c).

Administration of tocilizumab, a monoclonal antibody against the IL-6R, to patients with severe COVID-19 was reported to be either beneficial or neutral on disease outcome depending on the study design[36]. We collected blood samples from a cohort 2 of sCOVID-19 that received tocilizumab during the acute phase of the disease (n=10) and analyzed that data against patents that did not receive the drug (n=7). The administration of tocilizumab in cohort 2 was nearly random during the 2020 COVID-19 peak in New

York City, therefore no apparent clinical or demographic features influenced the analyses. Although we were unable to analyze the number of intact neutrophils in these samples, ACAL antibody titers (Fig. 5d), but not flagellin antibodies (Fig. 5d), were reduced in the convalescent plasma of tocilizumab-treated COVID-19 patients compared with patients who did not receive tocilizumab treatment. Notably, the increased transcription of genes encoding C-type lectin receptors (*CLEC7A, CLEC6A, CLEC4E*), downstream signaling molecules (*BCL10, MALT1, SYK, BAK1, BTK*) and antigen presentation (*HLA-B*, *HLA-DQ*, *CD74*, *B2M*, *IFI30*) was decreased in GMPs from recovering tocilizumab-treated patients compared to those without treatment (Fig. 5e and Extended Data Fig. 6a), suggesting that targeting the IL-6 pathway during sCOVID-19 had a positive impact on GMP transcriptional signatures and the decrease of ACAL titers. Together, this data indicated that IL-6 was a key mediator of the systemic immune effects exerted by gut *C. albicans* and might contribute to the immunopathology of sCOVID-19.

Interstitial lung changes in the acute stage of COVID-19 are associated with increased systemic neutrophils and markers of NET formation, suggesting a potential role for neutrophils in severe COVID-19 and potentially long COVID[33,37]. To assess whether intestinal fungi could influence the hyperinflammation in the lung in severe COVID-19, we used aged mice as a model of disease[38]. Twelve months old 129S1/SvImJ colonized with COVCa5 two weeks before infection with SARS-CoV-2 (Extended Data Fig. 6b) showed a significant increase of neutrophils in the peripheral blood 5 days post-SARS-CoV-2 infection compared to SARS-CoV-2-infected, non COVCa5-colonized mice (Fig. 5f). Furthermore, mature pulmonary Ly-6G$^+$CD11b$^+$ neutrophils that were MPO$^+$ and produced neutrophil extracellular traps (NETs) were observed more frequently in the lung of COVCa5 colonized mice that were infected with SARS-CoV-2 compared to non COVCa5-colonized, SARS-CoV-2-infected mice (Fig. 5g). Antifungal treatment with fluconazole (which targeted intestinal COVCa5) for two days after COVCa5 colonization for the duration of the experiment, decreased the numbers of circulating Ly-6G$^+$CD11b$^+$ neutrophil and NET formation in the lung compared to those of COVCa5-colonized mice without fluconazole (Fig. 5f, g). This finding aligns with current data in patients with candidemia[39]. This data suggested that expansion of gut *C. albicans* in sCOVID-19 patients could modulate neutrophil numbers and function in the blood and lungs.

DISCUSSION

Here we report that in addition to devastating secondary fungal infections in patients with severe pulmonary dysfunction[40], the mycobiota of the gastrointestinal tract might be a contributing factor to the immunopathology of severe COVID-19. High-resolution ITS-1-based sequencing survey, multiKAP and culture-dependent analysis indicated the presence of *C. albicans* in fecal samples from COVID-19 patients. Antifungal IgG antibody repertoire exploration detected increased titers of systemic IgG antibodies against *C. albicans* and other fungi associated with the gastrointestinal tract, but not toward commonly inhaled fungi, in patients with severe COVID-19. The analysis of hematopoietic stem cell progenitors in sCOVID-19 patients showed transcriptional alterations in pathways related to antifungal immunity and lasting reprogramming of GMPs, that were partially resolved upon targeting the IL-6 pathway with the drug tocilizumab. Mice colonized with *C. albicans* strains from

COVID-19 patients experienced increased ACAL IgG as well as lung neutrophilia and pulmonary NETosis during infection with SARS-CoV-2, which were partially resolved by antifungal treatment and by the blockade of IL-6.

A growing body of literature has reported how immune cell dysfunction contributes to the inflammatory response in patients with severe COVID-19[41], with microbiome-related factors also contributing to COVID-19 severity[42]. Our data suggested that the gut mycobiota could play a role in modulating the host immune response and could induce lasting immune alterations in the antifungal antibody response and the hematopoietic stem cell compartment in COVID-19 patients.

We observed that mature Ly-6G$^+$CD11b$^+$ neutrophils in the lungs of SARS-CoV-2-infected mice that were previously colonized with *C. albicans* exhibited enhanced production of MPO and enhanced release of NETs compared to the SARS-Cov-2 infected, non-*C.albicans* colonized mice. These observations suggested that *C. albicans* had an additional impact on neutrophils that amplified the detrimental effect of SARS-CoV-2 infection. This amplifying effect could be explained by the induction of fungal sepsis and/or the increased activation, maturation and overall numbers of neutrophils and their progenitors by fungal pathogen-associated molecular patterns (PAMPs). Fungal sepsis was reported in severe COVID-19 patients with an incidence of 1.6% to 4.4%[39,43]. Fungal PAMPs can enter the circulation during instance of gut barrier disturbance[9,44] and could potentially contribute to neutrophilia in severe cases of COVID-19, where the gut barrier function is compromised[45]. Hence, our findings suggest that gut-colonizing *C. albicans,* trough cell or fungal PAMPs translocation, could induce or amplify emergency hematopoiesis, reprogram GMPs and amplify the production of activated neutrophils, which could infiltrate the lungs and contribute to the severity of COVID-19. These findings are further supported by a study reporting an expansion of myeloid progenitors in the bone marrow of mice after intestinal colonization with *C. albicans*[46]. Similar mechanisms might be involved in other lung diseases, in which gut-activated fungal antigen-specific T_H17 cells have been observed in the lungs[11].

We showed that treatment with the antifungal drug fluconazole, which targeted intestinal *C. albicans*, reduced the number of circulating Ly-6G$^+$CD11b$^+$ neutrophil and inhibited NET formation in the lungs of COVCa5-colonized mice. This observation was consistent with reports indicating a potential therapeutic benefit of antifungal treatment in COVID-19 patients with candidemia[39] and underscored the modulatory effect of gut-colonizing *C. albicans* on neutrophil numbers and function. These observations could have implications regarding the potential therapeutic value of antifungal treatment, although future clinical studies are needed to determine causality.

IL-6 is a pleotropic cytokine with a variety of roles in the immune system that has been linked to tissue damage and immune cell activation in severe COVID-19[34,47]. Specifically, we found that systemic and lung neutrophilia prompted by intestinal *C. albicans* expansion were dependent on IL-6R. Myeloid signatures and increased numbers of circulating neutrophils in COVID-19 patients with severe respiratory disease are associated with NET formation and overall worse disease outcomes[48]. NETosis has been shown to contribute to tissue damage in pathophysiological conditions such as systemic lupus erythematosus

(SLE) and rheumatoid arthritis (RA)[49]. We found that the expansion of *C. albicans* in the intestine may contribute to the increase in lung neutrophil infiltration and NETosis in mice infected with SARS-CoV-2. Treatment of severe COVID-19 patients with an IL-6R blocking antibody led to a significant decrease in ACAL IgG and modulated the GMP expression of genes involved in antifungal immunity, which persisted for up to a year post IL-6R antibody treatment. This suggested that IL-6 may be involved in the long-lasting immune outcomes of post-COVID-19 inflammation, where gut fungi may also play a role. Our findings are consistent with the pleiotropic function of IL-6 on multiple cell types, including B cells, T cells, neutrophils and hematopoietic stem cell progenitors [34,50] and highlight the involvement of intestinal *C. albicans* blooms in the pathobiology of both local and systemic inflammation.

Altogether, out findings highlighted a mechanism by which gut fungal pathobionts might contribute to lasting immune alterations during inflammatory diseases and reprogramming of bone marrow progenitors and suggest the potential of mycobiota-immuno-based approaches to identify patients at risk for severe COVID-19 and long-lasting immune alterations.

METHODS

Human subjects.

Cohort 1.—Blood from 121 patients diagnosed with SARS-CoV-2 infection at Weill-Cornell Medicine (New York Presbyterian and Lower Manhattan hospitals) was collected under IRB 20-03021645 and IRB 20-03021671 between March 2020 and June 2020. Participants were recruited from the inpatient division of New York-Presbyterian Hospital and the Weill-Cornell Medicine pulmonary and post-ICU clinics. For 91 patients (25 mild/moderate and 66 severe) only blood samples were collected, allowing for measurement of fungal antibodies and calprotectin (Supplementary Table 1, Fig. 1, Fig. 3a, Extended Data Fig.1). For the rest of the COVID-19 patients of this cohort (30 patients divided into 17 mild/moderate and 13 severe), PBMCs were used for multidimensional flow cytometry as previously described[1] and measurement of fungal antibodies (Supplementary Table 1, Fig. 3b, c, Extended Data Fig. 3). All patients were classified as mild/moderate (mCOVID-19) and severe (sCOVID-19) disease according with oxygen requirements with mild/moderate disease defined as SARS-CoV-2 infection and <6 liters noninvasive supplemental oxygen to maintain SpO2 >92%, and severe disease defined as SARS-CoV-2 infection requiring hospitalization and received >6 liters supplemental oxygen or mechanical ventilation[1]. Blood samples from 36 SARS-CoV-2 negative individuals defined as by absence of clinical symptoms and negative for SARS-COV-2 Spike RBD IgG were used as ‘define control’ (HD, Supplementary Table 1, Fig. 1, Fig. 3a, Extended Data Fig. 1). Serum from 39 Crohn’s disease patients collected at Weill Cornell Medicine was used as CD ASCA positive controls. Antifungal antibodies were measured in plasma from all individuals. Throughout the study mild and moderate cases (mCOVID-19) were grouped together for analysis against severe cases (sCOVID-19) or uninfected subjects (HD) except in Figure 1a, where all COVID-19 patients were pulled together for comparison against CD patients and uninfected controls. Sample size was not statistically predetermined.

Clinical severity at the time of sample collection was assessed using the WHO eight-category ordinal scale: 1, not hospitalized and no limitations of activities; 2, not hospitalized, with limitation of activities, home oxygen requirement, or both; 3, hospitalized, not requiring supplemental oxygen and no longer requiring ongoing medical care (used if hospitalization was extended for infection-control or other nonmedical reasons); 4, hospitalized, not requiring supplemental oxygen but requiring ongoing medical care (related to COVID-19 or to other medical conditions); 5, hospitalized, requiring any supplemental oxygen; 6, hospitalized, requiring noninvasive ventilation or use of high-flow oxygen devices; 7, hospitalized, receiving invasive mechanical ventilation or extracorporeal membrane oxygenation (ECMO); and 8, death[3].

Cohort 2: Blood from patients diagnosed with SARS-CoV-2 infection at Weill-Cornell Medicine (New York Presbyterian and Lower Manhattan hospitals) was collected under IRB 20-03021645 and IRB 20-03021671 between March 2020 and March 2021. Participants were recruited from the inpatient division of New York-Presbyterian Hospital and the Weill-Cornell Medicine pulmonary and post-ICU clinics and as described in[4]. Samples form total of 39 subjects including healthy volunteers (HD, defined as by absence of clinical symptoms and negative for SARS-COV-2 Spike RBD IgG) , recovered severe COVID-19 patients (WHO score 6-7, sCOVID-19), and recovered non-COVID-19 critically ill patients (non-COVID19) were used for plasma and $CD34^+$ cell isolation (Supplementary Table 2). Twenty six of these 39 subjects were followed after recovery from mild/moderate (mCOVID-19) or severe (sCOVID-19) COVID-19 and were partitioned into an early recovery group (2-4 months following admission, “Early”) and a late recovery group (4-12 months following admission, “Late”) as described in[4].

Cohort 3—consisted of 10 COVID-19 patients treated as inpatients at Weill Cornell Medicine NewYork-Presbyterian Hospital, between January and April 2021. Sample size was not statistically predetermined. Blood and fecal samples were collected under IRB 20-03021645. Ten SARS-CoV-2 negative individuals defined as by absence of clinical symptoms were used as uninfected controls (HD). Clinical severity at the time of fecal sample collection was assessed using the WHO eight-category ordinal scale as above.

Human sample processing and gut fungal strain isolation.—Patient samples were handled under Biosafety Level 2^+ containment conditions following risk assessments and code of practice approved by Weill-Cornell Medicine. Blood samples in serum separator tubes were centrifuged at 1,500g for 10 min and serum aliquoted and stored at −80 °C. Aliquots of blood from heparin tubes were stained for whole-blood flow cytometry panels (see Flow cytometry section) or centrifuged at 2,000g for 10 min and plasma stored at −80 °C. Fresh human fecal samples collected from COVID-19 patients were diluted in sterile PBS and plated onto Sabouraud dextrose agar (SDA), supplemented with penicillin/streptomycin (Sigma). SDA plates were incubated at 37 °C for 48 hours. Fungal colonies were picked up from both cultures (37 °C, overnight). Isolated fungal colonies from each individual subject were identified by matrix-assisted laser desorption/ionization-time of flight (MALDI-TOF) mass spectrometer. *Candida albicans* COVCa1, *C. albicans* COVCa2, *C. albicans* COVCa5 and *C. glabrata* COVCg3 were used in this study.

Fungal lysates preparation.—*Candida albicans* SC5314 (ATCC® MYA76™), *Saccharomyces cerevisiae* (ATCC® MYA-796™), *Candida parapsilosis* (ATCC® 22019™), *Aspergillus fumigatus Fresenius* (ATCC® 46645™), and *Malassezia restricta* (ATCC® MYA-4611™) were obtained from the American Type Culture Collection (ATCC). *Candida albicans, Candida parapsilosis, Saccharomyces cerevisiae* were first grown on SDA plates, and then cultivated in Sabouraud Dextrose Broth (SDB; EMD Chemicals) at 37°C in aerobic conditions overnight. *Aspergillus fumigatus* was collected after 4 days of growth on SDA plates at 30°C and germinated in liquid media until mycelia were present. *Malassezia restricta* was cultured on modified Dixon agar plates and cultivated in modified Dixon medium for 7 days. *Candida albicans*, *Candida parapsilosis*, *Saccharomyces cerevisiae*, and *Malassezia restricta* were harvested by centrifugation for 5 min at 330g. Mycelia of *Aspergillus fumigatus* were collected in filter paper.

For fungal lysate preparation, all fungal pellets were washed three times with PBS (Corning), fixed in 4% paraformaldehyde for 60 min at 4°C. Fungal suspensions were washed 3 times by pelleting at 900g for 2 min, aspirating the supernatant, and resuspending the pellet in molecular-grade water. They were treated with three freeze-thaw cycles of 10 minutes in dry ice, then 10 min in a 75°C incubator. Finally, fungal suspensions were sonicated for eight cycles of 15 seconds on/ 30 seconds off for cell disruption. All extracts were centrifuged at 15,000g for 10 min to remove debris and supernatants were stored at −30°C until use for ELISA plate coating. The extract of *Alternaria alternata* was obtained from Greer Laboratories. The extract was resuspended in PBS, centrifuged at 15,000g for 10 min and supernatants were stored at −30°C until use.

ELISA.—Recombinant SARS-CoV-2 Receptor Binding Domain (RBD) protein and recombinant SARS-COV-2 Spike RBD protein antibody were obtained from Abclonal. To measure the antibody against fungi, fungi lysates or yeast mannan (Sigma) were used as the coating antigen. 96-well plates (Corning) were coated with 1μg/mL of recombinant SARS-CoV-2 protein, 0.5 ng/mL of flagellin (Invivogen), 2.5 μg/mL of yeast mannan from Saccharomyces cerevisiae (Sigma) or 1 μL of fungi lysates (10^9 fungi/mL) in carbonate coating buffer and incubated at 4°C. Next, plates were washed 3 times with PBS containing 0.05% Tween 20 (Wash Buffer) and blocked with 1% BSA in PBS with 0.02% Tween-20 (PBS-T) for 1h at room temperature. All samples were diluted at 50-2000-fold dilutions followed by serial dilutions by 3 in 1% BSA PBS-T, incubated for 2 hours at room temperature. Plates were washed 3 times with Wash Buffer. Thereafter anti-human IgG-HRP or anti-mouse IgG-HRP (Southern Biotech) were diluted in 1% BSA in PBS-T at 1:4,000 and incubated for 1h. Plates were washed 5 times with Wash Buffer, developed by the chromogenic substrate 3,3’,5,5’-tetramethylbenzidine (TMB) solution (BD Bioscience). The reaction was quenched with 2M sulfuric acid. Plates were read on a plate reader (SpectraMax Plus 384 Microplate Reader, Molecular devices) at 450 and 570nm, and ODs were background subtracted. Endpoint titers were plotted for each specimen and an ODs, more than one third of maximum ODs, was considered a positive readout. Human and mouse calprotectin were quantified using BioLegend and R&D ELISA kits according to manufacturer’s instructions, respectively.

Mice.—5-7-week-old wildtype (WT) C57BL/6J mice were originally obtained from the Jackson Laboratories. Mice were bred and maintained under specific pathogen-free (SPF) conditions. All Animal care and experimental protocols were performed in accordance with the institutional animal care and use committee of Weill Cornell Medicine and Icahn School of Medicine at Mount Sinai. To establish *C. albicans* intestinal colonization in vivo experiments, mice were given drinking water supplemented with an antibiotic cocktail [0.4 g/L ampicillin, 0.4 g/L vancomycin (Gold Biotechnology), 0.4 g/L cefoperazone (Sigma)] two days prior to oral fungi colonization and continued throughout the entirety of the experiment. For intestinal fungi colonization, fungi were grown as described above, then washed and resuspended at a concentration of $2.5x10^8$ fungi/mL of PBS. Mice were orally gavaged with $5x10^7$ CFU/mouse at the times indicated. To quantify fungi burden in the gut, feces were collected and suspended into PBS, serially diluted and plated on SDA plates. After an overnight incubation at 37°C in an anaerobic chamber, CFUs of fungi were counted and normalized to stool weight. For anti-fungal treatment, 0.5 g/L of fluconazole water (Sigma) was provided to mice *ad libitum* two days after colonization for the duration of the experiment. In the IL-6R blockade experiments, 200 μg of InVivoMAb anti-IL-6R (15A7; BioXCell) or InVivoMAb isotype control, anti-trinitrophenol (2A3; BioXcell) was administered through intraperitoneal injection every other day for the duration of the experiment. One year old 129S1 mice were purchased from Jackson laboratories and housed under SPF conditions. Infection with SARS-CoV-2 was performed at the Icahn School of Medicine at Mount Sinai. ABX-treated and COVCa-colonized or non-colonized 12-month-old female mice were infected intranasally with 1×10^4 PFU hCoV-19/USA (Beta, B.1.351) in 50 μL of PBS under mild Ketamin/Xylazin sedation. On day 4 after infection, animals were killed, and tissue specimens were collected for analyses.

Isolation of cells from colonic lamina propria (cLP), lung and blood.—Colonic lamina propria cells were isolated as previously described[2,6]. The middle and superior lobes of the right lung were harvested after perfusion and minced, then placed for 45 min at 37°C in 5 ml a RPMI medium containing 5% FBS, liberase (100 μg/ml; Roche) and deoxyribonuclease type 1 (DNase I) (50 μg/ml; Sigma), 100 IU/ml penicillin and 100 μg/ml streptomycin (Thermo Fisher Scientific). The cells were recovered by disruption through a 100-μm nylon cell strainer before being centrifuged at 300g for 5 min. Lysis of red blood cells was performed for 2 min at room temperature before a final centrifugation at 300g for 5 min and resuspension of the remaining cell pellet in 2 ml of PBS containing 1% BSA.

Blood samples were harvested by cardiac puncture from a euthanized mouse. Cell suspensions were washed with RBC lysis Buffer (BioLegend), then centrifuged and resuspended in PBS containing 1% fetal bovine serum.

Flow cytometry.—High-dimensional immune cell profiling of circulating blood of COVID-19 patients was performed as described[1]. In brief, human peripheral blood was collected in Na-heparin. Polymorphonuclear leukocytes and monocytes were collected by density gradient centrifugation of PBMCs, erythrocytes were lysed with BD Pharm Lyse. Peripheral blood was washed in PBS, lysed in 1× BD Pharm Lyse, and washed again in PBS. PBMC cell suspensions were prepared with Ficoll-Paque following the manufacturer's

protocol. Cells were stored briefly in storage media (10% FBS/1% L-glutamine/1% pen-strep) before staining with antibody cocktails for flow cytometry. Cells were washed with PBS and then stained with dead cell dye (Fixable Viability Stain 700; BD Horizon) before washing with wash buffer (0.5% BSA/DPBS/NaN_3). Cells were then treated with 50 μl of Fc-blocking solution (2% normal rabbit serum/10% BD Fc Block/PBS) before application of a 100-μl antibody cocktail diluted in wash buffer. Samples were stained within 6 h of sample collection and analyzed on a BD Biosciences FACSCanto (BD Bioscience) flow cytometer within 2 h of staining. Analysis was performed using BD FACSDiva software. Fluorophore conjugated antibodies were used as follows: FITC-Cy7 anti-CD158e (NKB1) (DX9) (BD Pharmingen), PE anti-CD158b (CH-L) (BD Pharmingen), PerCP-Cy5.5 anti-CD158a (/h/g) (HP-MA4) (Invitrogen), PE-Vio770 anti- CD159a (NKG2A) (REA110) (Miltenyi Biotec), APC anti-CD158i (KIR2DS4) (JJC11.6) (Miltenyi Biotec), APC-H7, PE-Cy7 and FITC anti-CD3 (SK7 (Leu-4)) (BD Biosciences), BV421 anti-CD56 (NCAM16.2) (BD Horizon), V500C anti-CD45 (2D1) (BD Biosciences), BV605 anti-CD16 (3G8) (BD Horizon), PE-Cy7 anti-CD19(J3-119) (Beckman Coulter / Immunotech), PE-Cy7 anti-CD56 (N901(NKH-1)) (Beckman Coulter / Immunotech), APC anti-CD11b (D12) (BD Biosciences), APC-H7 anti-CD14 (MphiP9) (BD Biosciences), CD124 anti-CD124 (G077F6) (BioLegend), APC-H7 anti-CD8 (SK1) (BD Biosciences), PE-Cy7 anti-CD4 (SK1) (BD Biosciences), BV421 anti-CD19 (HIB19) (BD Horizon), BV605 anti-CD5 (UCHT2) (BD Horizon), and APC-H7 anti-CD20 (L27) (BD Biosciences).

Fecal material was prepared by dilution and homogenization in cold sterile PBS at 25 mg/mL and strained through a 70μm-nylon mesh cell strainer. For intestinal lavage normalization, samples were centrifuged at 900g for 10 min, after which supernatant was transferred to a separate tube, pelleted dry weight was recorded and then resuspended at 25 mg dry weight per mL supernatant, supplementing additional volume as necessary with cold sterile PBS. 50 μL of filtered fecal samples were conducted by centrifugation and resuspended in 100 μL of 4% PFA for 1 hour at 4°C. Samples were again centrifuged and aspirated, then resuspended in 100 μL of staining buffer containing both 500 fold dilution of calcofluor white (CFW; Sigma,18909-100ML-F) and 1,000 fold dilution of SybrGreen (Sybr;Thermo Fisher Scientific, S7563) for 45 min at 4°C. Samples were prepared for flow cytometry by resuspension in 150 μL FACS buffer (1% PFA/0.05% sodium azide) and storage at 4°C.

Mouse flow cytometry analysis was performed as described[5,6]. Cell suspensions of murine cells were prepared as described above, stained with different combinations of fluorochrome-conjugated antibodies in the presence of Purified Rat Anti-Mouse CD16/CD32 (BD Biosciences). Fixable Viability Dye eFluor 506 (Thermo Fisher Scientific) was used to exclude dead cells. After incubation at 4°C for 30 min, cells were washed with FACS buffer, pelleted by centrifugation, and resuspended in 200 μL of FACS buffer. Data was acquired on LSR Fortessa (BD Bioscience). Flow cytometry analysis was performed by using FlowJo (TreeStar) software using a uniform sequential gating strategy (Extended Data Fig. 2a.b). Flow cytometry data was shown as mean fluorescence intensity. Fluorophore conjugated antibodies were used as follows: BUV395 anti-CD11b (M1/70) (BD Bioscience), BV605 anti-CD4 (RM4-5) (BioLegend), BV650 anti-CD45 (30-F11)

(BioLegend), BV711 anti-Ly-6G (1A8) (BioLegend), and APC-Cy7 anti- TCRβ (H57-597) (BioLegend).

Immunofluorescence staining.—Tissues were processed as previously described[7,8]. Lung tissues were fixed for 48 h in 4%paraformaldehyde at 4°C. Two days later, tissues were dehydrated in 30% sucrose overnight at 4°C and subsequently embedded in optimal cutting temperature compound (OCT) media. Frozen tissue sections were sectioned using Leica CM1850/Leica 3050S at a thickness of 20 μm. Fc receptors were blocked with anti-CD16/32 Fc block antibody (BioLegend) diluted in PBS containing 2% serum and 2% FBS for 1 hour at room temperature. Sections were stained with the antibodies; Donkey anti-goat MPO (R&D System), Goat anti-rabbit Histone H3 (abcam), APC anti-Ly-6G (1A8) (BioLegend) were diluted in PBS containing 2% donkey serum, 2% FBS, and 0.05% FC Block for 1 hour at room temperature. Sections were subsequently washed with 1xPBS and counter stained with donkey anti-goat 488 (Invitrogen) and donkey anti-rabbit 555 (Invitrogen). Sections were cover slipped using Immun-mount mounting medium (Fisher Scientific) and Cover Glasses with a 0.13 to 0.17 mm thickness (Fisher Scientific). Fluorescence was detected with a Zeiss LSM 880 confocal microscope (Carl Zeiss) equipped with 405, 488, 514, 561, 594, and 633 nm solid-state laser lines, a 32-channel spectral detector (409-695 nm), and 10x0.3, 20x Plan-Apochromat 0.8, 40x, and 6331.40 objectives. Zen Black (Carl Zeiss) software suite was used for data collection. The imaging data were processed and analyzed using Imaris software version 8.3.1 (Bitplane USA). Image analysis was conducted on acquired images as follows: two sections per slide, and two slides per animal of n = 4-6 animals.

Mycobiota library generation, sequencing, and analysis.—DNA was extracted from homogenized human fecal samples using DNA HiBind mini spin columns Kit (Omega) according to manufacturer's instructions. Fungal ITS1 sequencing, and analysis has been performed as previously described [6,9].

CD34$^+$ cell isolation and single-cell RNA and ATAC sequencing.—CD34$^+$ cell isolation and single-cell library preparation was performed as previously described[4]. Frozen peripheral blood mononuclear cells (PBMCs) were thawed in a 37°C water bath and subsequently washed with RPMI before being centrifuged. An aliquot of the PBMCs was stained with 7-AAD (Biolegend) alone for viability assessment. The remaining cells were incubated with CD34 microbeads (Miltenyi) and isolated using a magnetic column (Miltenyi) following the manufacturer's instructions. The positively-selected cells were then stained with a panel of antibodies including FITC anti-CD34 (AC136) (Miltenyi), Pacific Blue anti-CD49f (Biolegend)(GoH3), PE anti-CD90 (5E10) (Biolegend), PE/cy7 anti-CD38 (HIT2) (Biolegend), APC/cy7 anti-CD45RA (HI100) (Biolegend) and lineage markers (Biotin anti-CD20 (2H7) , Biotin anti-CD3 (SK7), Biotin anti-CD16 (3G8), Biotin anti-CD56 (5.1H11) and Biotin anti-CD14 (M5E2), (Biolegend)). After incubating in the dark for 30 minutes, the cells were washed with PBS and subsequently incubated with Streptavidin-BV605 (BD) for another 30 minutes. CD34+ cells were then sorted from the positive fraction, and viable PBMCs were sorted from the PBMC aliquot using a BD FACSAria cell sorter at ratios of 1:5-1:20. Nuclei were isolated from a mix of CD34+

cells and PBMC according to ‘Low Cell Input Nuclei Isolation’ protocol (10x Genomics CG000365-Rev B) and were processed using Chromium Controller & Next GEM Accessory Kit (10x Genomics 1000202) and Chromium Next GEM Single Cell Multiome ATAC+ Gene Expression Reagent Bundle (10x Genomics 1000285) following the manufacturer’s User Guide (10x Genomics CG000338-Rev D). Targeted nuclei recovery ranged from 5,000 to10,000. The single-cell RNA and ATAC sequencing libraries were prepared using Dual Index Kit TT Set A (10x Genomics 1000215) and Single Index Kit N Set A (10x Genomics 1000212) respectively and sequenced on Illumina NovaSeq6000 or NextSeq platform. The data analysis were performed as described[4]. The data is available on GEO database under accession number GSE196990.

Quantification and statistical analysis.—Statistics were computed using GraphPad Prism version 8.4.3 (GraphPad Software). In general, non-parametric Mann-Whitney Wilcoxon test (which does not assume normal distribution) was used for two groups and one-way ANOVA with Tukey’s or Kruskal-Wallis and Dunn’s for multiple comparisons was used for three or more groups. Statistical details specific to experiments are reported in the figure legends. Graphs display mean values with error bars that correspond to the standard error of the mean (mean ± SEM). Statistical analysis on mycobiome-related data was performed using R version 4.0.4 (R Core Team, 2014). The P value(s) reported in the figure legends are the likelihood(s) of observing the effect size(s) if the null hypothesis of zero difference is true. They are denoted as: not significant (ns) $p \geq 0.05$, *$p < 0.05$, **$p < 0.01$, ***$p < 0.001$, ****$p < 0.0001$. Analysis of cell frequencies and antibody levels: Correlations between cell frequencies and anti-*Candida albicans* antibody (ACAL IgG) levels and flow cytometry-derived cellular data were assessed within groups of severe (n=13) or low to moderate (n=17) COVID-19 patients using the Spearman correlation coefficient and associated statistical test. Differing correlations between severe versus mild/moderate groups were assessed by evaluating the significance of an interaction term in the linear model cell.frequency ~ antibody.level + severity + antibody.level:severity. Statistical analysis was performed using R version 4.0.4 (R Core Team, 2014) and associated plots generated using ggplot2 (Wickham 2016).

Extended Data

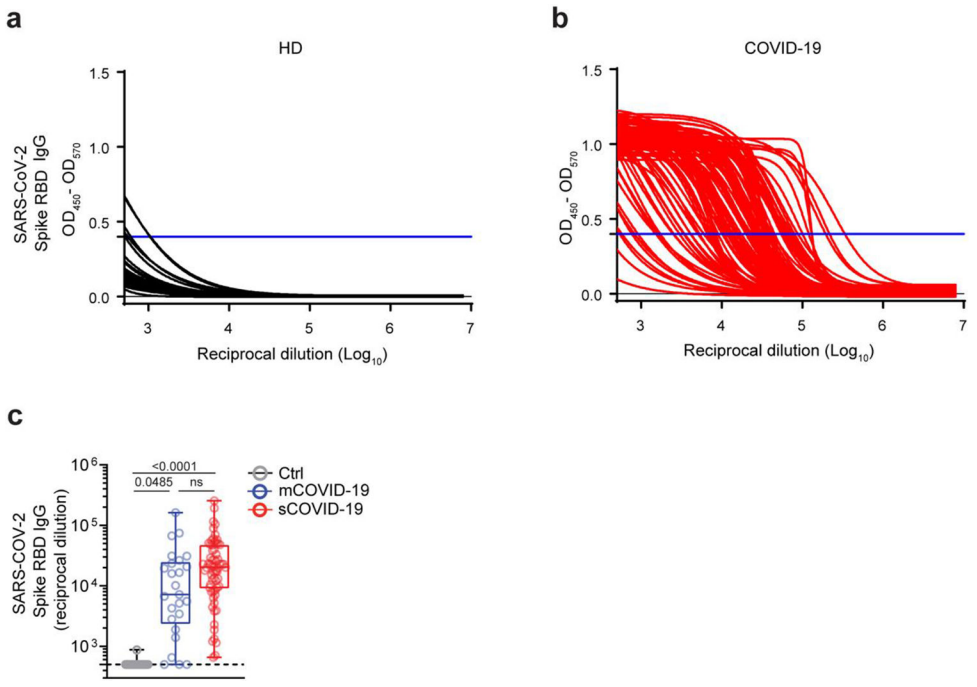

Extended Data Fig.1. Serological testing in Cohorts 1 and 2.

a-b, SARS-CoV-2 RBD IgG titration curves in HD (n=36, **a)** and sCOVID-19 (n=66, **b).** **c,** Plasma IgG antibody titers to SARS-CoV-2 RBD in HD (n=36), mCOVID-19 (n=25) and sCOVID-19 (n=66) (Supplementary Table. 1). The data are shown as endpoint titers normalized to ELISA reciprocal dilution as in a and b. The dotted line indicates the limit of detection. In the boxplots, the center is drawn through the median of the measurement, and the lower and upper bounds of the box correspond to the first and third quartile. The whiskers go down to the smallest value and up to the largest. Statistical significance was determined by the one-way ANOVA followed by Tukey's multiple-comparison. Related to Figure 1

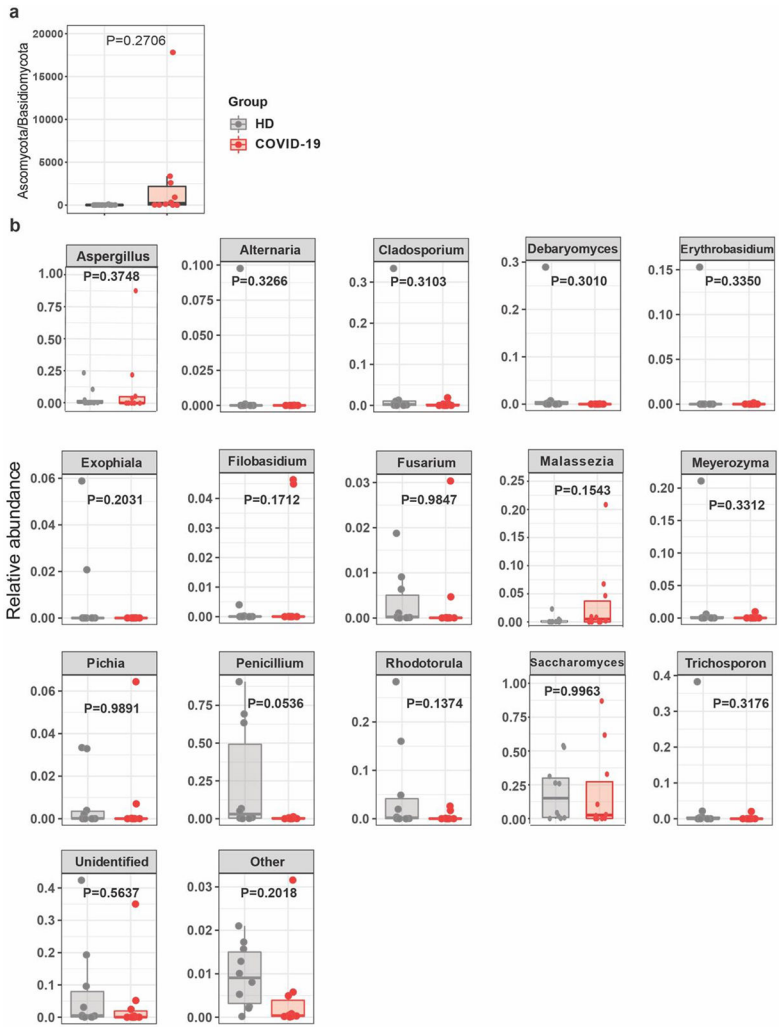

Extended Data Fig.2. Compositional analysis of gut mycobiota.

a-b, Ratio between Ascomycota and Basidiomycota **(a)** and relative abundance of fungal species **(b)** in ITS1 sequencing of fungal rDNA from stool samples of HD (n=10) and COVID-19 patients (n=10). Lower and upper hinges correspond to the first and third quartile; dots represent individual patients' samples. P values were calculated using a two-tailed Mann-Whitney testing between all groups. Related to Figure 2.

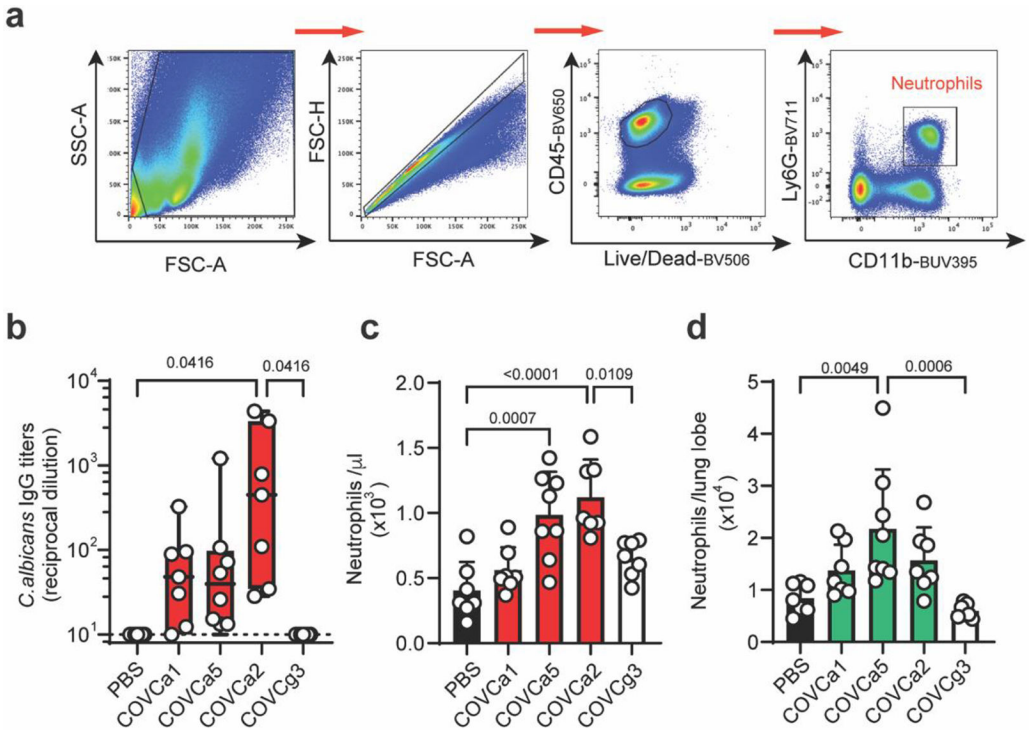

Extended Data Fig.3. Immune responses to *C.albicans* isolates from COVID-19 patients.

a, Representative graphs depicting the flow cytometry gating strategy for defining murine neutrophil populations in tissues. **b-d**, Anti-*C. albicans* specific IgG titers (**b**), the amount of neutrophils in peripheral blood (**c**) and lung (**d**) in antibiotic-treated mice orally gavaged or not (PBS, n=7) with either *C. glabrata* (CgCOV3, n=7) or *C. albicans* (CaCOV1, CaCOV5, CaCOV2, n=7) isolated from COVID-19 patient's stool . Immune responses were assessed at 2 weeks after colonization. In boxplots in b, the center is drawn through the median of the measurement, and the lower and upper bounds of the box correspond to the first and third quartile. The whiskers go down to the smallest value and up to the largest. The bar graphs in c and d presented as mean ± SEM. The results were pooled from two experiments. P values were calculated using the one-way ANOVA followed by Tukey's multiple comparison. ns=not significant. Related to Figures 2 and 3.

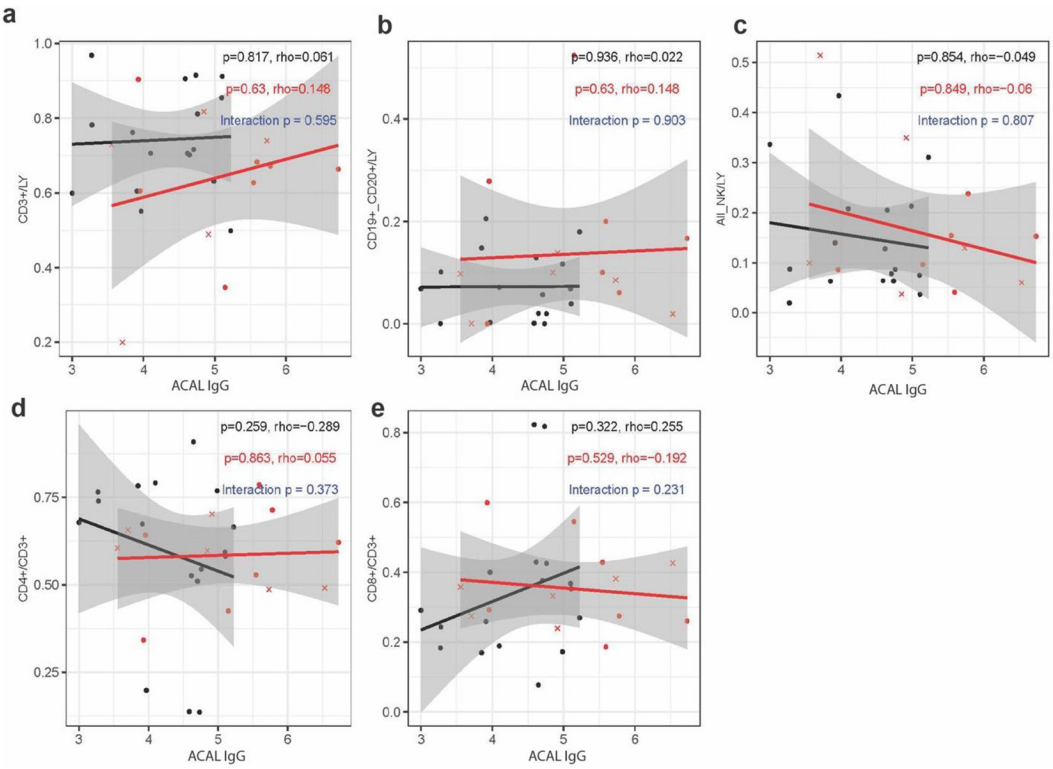

Extended Data Fig.4. Linear regression analysis of the Immune cell frequencies and levels of ACAL IgG in peripheral blood of mCOVID-19 and sCOVID-19 s.

a-e, Comparison of linear regression analysis of $CD3^+$ T cell (**a**), $CD19^+CD20^+$ B cell (**b**), NK cell (**c**), $CD4^+$ T cell (**d**) and $CD8^+$ T cell (**e**) frequencies and levels of ACAL IgG in peripheral blood of sCOVID-19 (n=13) and mCOVID-19 (n=17), see Supplementary Table 1. Crosses indicate deceased patients. Red and black lines show linear fits within severe and low to moderate groups, respectively, with 95% confidence intervals shown in gray. Spearman correlation estimates (rho) and associated p values are shown in red and black for sCOVID-19 and mCOVID19, respectively. Related to Figure 3.

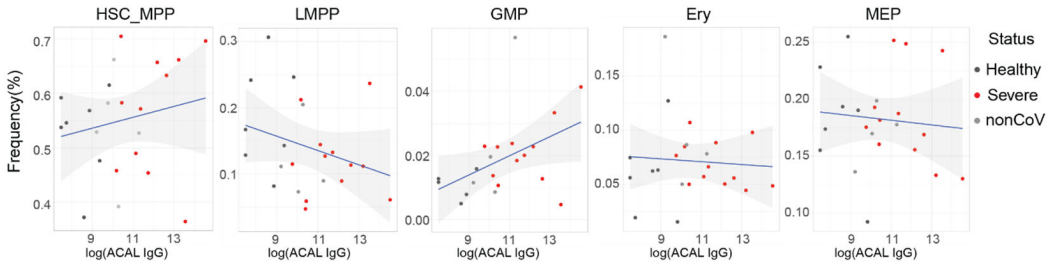

Extended Data Fig.5. Strong correlation between ACAL IgG and GMPs among multiple progenitor cell types.

Correlation and linear regression of frequency of hematopoietic stem cells/multipotent progenitor cells (HSC/MPP), lymphoid-primed multipotent progenitor cells (LMPP), granulocyte-macrophage progenitor cells (GMP), erythroid progenitor cells (Ery), megakaryocyte-erythroid progenitor cells (MEP) with ACAL IgG (log10 titer) in enrichment of $CD34^+$ HSPC from PBMC of HD(n=5), sCOVID-19 (n=12) and nonCOV-19 (n=5),

see Supplementary Table 2. Blue line indicates the regression line for all patients. The associated linear regression equation, Pearson's correlation. Coefficient, and significance are shown. Related to Figure 4.

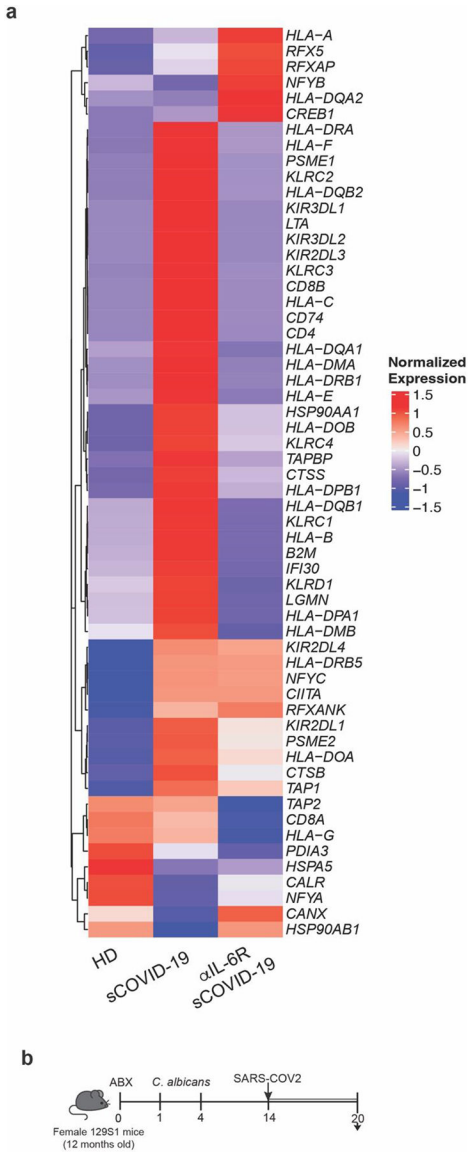

Extended Data Fig.6. HLA-related transcriptional signatures of GMPs form HD, sCOVID19 and sCOVID19 treated with tocilizumab.

a, Heatmap showing antigen presentation marker that are differentially expressed in GMP of HD(n=7) and sCOVID-19 who received(n=6) or not (n=7) IL-6R blockade treatment. Data are average of normalized expression for each gene in each group. **b,** Antibiotic treated mice were colonized with *C.albicans* CaCOV5 by oral gavage twice for two weeks prior to SARS-COV-2 challenge and were harvested at Day 20. Water with or without antifungal fluconazole was provided to mice two days after second oral gavage. Related to Figure 5.

Supplementary Material

Refer to Web version on PubMed Central for supplementary material.

Acknowledgments

We thank members of the Iliev laboratory for their critical reviews of the manuscript. We thank all contributing members of the Department of Pathology and Laboratory Medicine, of the JRI IBD Live Cell Bank Consortium, and the Microbiome Core Laboratory of Weill Cornell Medicine, the NYU Langone Health Microscopy Laboratory (NCI P30CA016087), Khanna laboratory (supported by R01AI143861 and R01AI143861-02S1) and Randy Albrecht, Richard Cadogan, Daniel Flores for support with the BSL3 facility and procedures. M.S was supported by R01AI160706, R01DK130425. AGS was supported by CRIPT, CEIRR (contract # 75N93021C00014) and by the US National Institutes of Health (U19AI135972, U19AI168631 and U19AI142733). Research in the Iliev laboratory is supported by US National Institutes of Health (DK113136, DK121977 and AI137157), the Leona M. and Harry B. Helmsley Charitable Trust, the Irma T. Hirschl Career Scientist Award, Crohn's and Colitis Foundation, and the Burrough Welcome Trust PATH Award. I.D.I is a fellow of the CIFAR program Fungal Kingdom: Threats and Opportunities.

Data availability

16S and ITS sequencing data are available in the NCBI Sequence Read Archive (SRA) with the accession code PRJNA732432. The single-cell transcriptome and ATAC sequencing data have been deposited in NCBI Gene Expression Omnibus (GEO) under the accession number GSE196990. Source data are provided with this paper.

REFERENCES

1. COVID-19 Dashboard. the Center for Systems Science and Engineering (CSSE) at Johns Hopkins University (JHU).
2. Guan W-J, et al. Clinical Characteristics of Coronavirus Disease 2019 in China. New England Journal of Medicine 382, 1708–1720 (2020). [PubMed: 32109013]
3. Al-Aly Z, Bowe B & Xie Y Long COVID after breakthrough SARS-CoV-2 infection. Nature Medicine 28, 1461–1467 (2022).
4. Lucas C., et al. Longitudinal analyses reveal immunological misfiring in severe COVID-19. Nature 584, 463–469 (2020). [PubMed: 32717743]
5. Lau RI, et al. Gut microbiota in COVID-19: key microbial changes, potential mechanisms and clinical applications. Nature Reviews Gastroenterology & Hepatology (2022).
6. Miyauchi E, Shimokawa C, Steimle A, Desai MS & Ohno H The impact of the gut microbiome on extra-intestinal autoimmune diseases. Nature Reviews Immunology (2022).
7. Hou K., et al. Microbiota in health and diseases. Signal Transduction and Targeted Therapy 7(2022).
8. Liu Q., et al. Multi-kingdom gut microbiota analyses define COVID-19 severity and post-acute COVID-19 syndrome. Nature Communications 13(2022).
9. Arunachalam PS, et al. Systems biological assessment of immunity to mild versus severe COVID-19 infection in humans. Science, eabc6261 (2020).
10. Li XV, Leonardi I & Iliev ID Gut Mycobiota in Immunity and Inflammatory Disease. Immunity 50, 1365–1379 (2019). [PubMed: 31216461]
11. Bacher P., et al. Human Anti-fungal Th17 Immunity and Pathology Rely on Cross-Reactivity against *Candida albicans*. Cell 176, 1340–1355.e1315 (2019). [PubMed: 30799037]
12. Leonardi I., et al. $CX3CR1^{+}$ mononuclear phagocytes control immunity to intestinal fungi. Science 359, 232–236 (2018). [PubMed: 29326275]
13. Salmanton-García J., et al. COVID-19–Associated Pulmonary Aspergillosis, March–August 2020. Emerging Infectious Disease journal 27, 1077 (2021).

14. Zuo T., et al. Alterations in Fecal Fungal Microbiome of Patients With COVID-19 During Time of Hospitalization until Discharge. Gastroenterology 159, 1302–1310.e1305 (2020). [PubMed: 32598884]
15. Lv L., et al. Gut mycobiota alterations in patients with COVID-19 and H1N1 infections and their associations with clinical features. Communications Biology 4, 480 (2021). [PubMed: 33850296]
16. Standaert–Vitse A., et al. Candida albicans Is an Immunogen for Anti Saccharomyces cerevisiae Antibody Markers of Crohn's Disease. Gastroenterology 130, 1764–1775 (2006). [PubMed: 16697740]
17. Wang ZZ, Shi K & Peng J Serologic testing of a panel of five antibodies in inflammatory bowel diseases: Diagnostic value and correlation with disease phenotype. Biomed Rep 6, 401–410 (2017). [PubMed: 28413638]
18. Sokol H., et al. Fungal microbiota dysbiosis in IBD. Gut 66, 1039–1048 (2017). [PubMed: 26843508]
19. Brown GD, et al. Hidden Killers: Human Fungal Infections. Science Translational Medicine 4, 165rv113–165rv113 (2012).
20. Koutsakos M., et al. Integrated immune dynamics define correlates of COVID-19 severity and antibody responses. Cell Reports Medicine 2(2021).
21. Hoenigl M., et al. COVID-19-associated fungal infections. Nature Microbiology 7, 1127–1140 (2022).
22. Proctor DM, et al. Integrated genomic, epidemiologic investigation of Candida auris skin colonization in a skilled nursing facility. Nature Medicine 27, 1401–1409 (2021).
23. Leonardi I., et al. Fungal Trans-kingdom Dynamics Linked to Responsiveness to Fecal Microbiota Transplantation (FMT) Therapy in Ulcerative Colitis. Cell Host & Microbe 27, 823–829.e823 (2020). [PubMed: 32298656]
24. Zhai B., et al. High-resolution mycobiota analysis reveals dynamic intestinal translocation preceding invasive candidiasis. Nature Medicine 26, 59–64 (2020).
25. Doron I., et al. Human gut mycobiota tune immunity via CARD9-dependent induction of anti-fungal IgG antibodies. Cell 184, 1017–1031.e1014 (2021). [PubMed: 33548172]
26. Li X., et al. Response to Fungal Dysbiosis by Gut-Resident CX3CR1^{+} Mononuclear Phagocytes Aggravates Allergic Airway Disease. Cell Host & Microbe 24, 847–856.e844 (2018). [PubMed: 30503509]
27. Li XV, et al. Immune regulation by fungal strain diversity in inflammatory bowel disease. Nature (2022).
28. Silvin A., et al. Elevated Calprotectin and Abnormal Myeloid Cell Subsets Discriminate Severe from Mild COVID-19. Cell 182, 1401–1418.e1418 (2020). [PubMed: 32810439]
29. Rendeiro AF, et al. Profiling of immune dysfunction in COVID-19 patients allows early prediction of disease progression. Life Science Alliance 4, e202000955 (2021). [PubMed: 33361110]
30. Mann ER, et al. Longitudinal immune profiling reveals key myeloid signatures associated with COVID-19. Science Immunology 5, eabd6197 (2020). [PubMed: 32943497]
31. Shao TY, et al. Commensal Candida albicans Positively Calibrates Systemic Th17 Immunological Responses. Cell Host Microbe 25, 404–417 e406 (2019). [PubMed: 30870622]
32. Al-Aly Z, Xie Y & Bowe B High-dimensional characterization of post-acute sequelae of COVID-19. Nature 594, 259–264 (2021). [PubMed: 33887749]
33. George PM, et al. A persistent neutrophil-associated immune signature characterizes post-COVID-19 pulmonary sequelae. Science Translational Medicine 14, eabo5795 (2022). [PubMed: 36383686]
34. Cheong J-G, et al. Epigenetic memory of coronavirus infection in innate immune cells and their progenitors. Cell 186, 3882–3902.e3824 (2023). [PubMed: 37597510]
35. Leonardi I., et al. Mucosal fungi promote gut barrier function and social behavior via Type 17 immunity. Cell 185, 831–846.e814 (2022). [PubMed: 35176228]
36. Rosas IO, et al. Tocilizumab in Hospitalized Patients with Severe Covid-19 Pneumonia. New England Journal of Medicine 384, 1503–1516 (2021). [PubMed: 33631066]
37. Zuo Y., et al. Neutrophil extracellular traps in COVID-19. JCI Insight 5(2020).

38. Dinnon KH, et al. A mouse-adapted model of SARS-CoV-2 to test COVID-19 countermeasures. Nature 586, 560–566 (2020). [PubMed: 32854108]
39. Çavuş MA & Sav H Opportunistic Infections in Critical COVID-19 Patients. Polish Journal of Microbiology 71, 411–419 (2022). [PubMed: 36185025]
40. Hoenigl M., et al. The emergence of COVID-19 associated mucormycosis: a review of cases from 18 countries. The Lancet Microbe 3, e543–e552 (2022). [PubMed: 35098179]
41. Bastard P., et al. Autoantibodies against type I IFNs in patients with life-threatening COVID-19. Science 370, eabd4585 (2020). [PubMed: 32972996]
42. Yeoh YK, et al. Gut microbiota composition reflects disease severity and dysfunctional immune responses in patients with COVID-19. Gut 70, 698–706 (2021). [PubMed: 33431578]
43. Kayaaslan B., et al. Incidence and risk factors for COVID-19 associated candidemia (CAC) in ICU patients. Mycoses 65, 508–516 (2022). [PubMed: 35156742]
44. Giron LB, et al. Markers of fungal translocation are elevated during post-acute sequelae of SARS-CoV-2 and induce NF-κB signaling. JCI Insight 7(2022).
45. Sun Z., et al. Gut microbiome alterations and gut barrier dysfunction are associated with host immune homeostasis in COVID-19 patients. BMC Medicine 20(2022).
46. Chen Y-H, et al. Rewilding of laboratory mice enhances granulopoiesis and immunity through intestinal fungal colonization. Science Immunology 8, eadd6910 (2023). [PubMed: 37352372]
47. McGonagle D, Sharif K, O'Regan A & Bridgewood C The Role of Cytokines including Interleukin-6 in COVID-19 induced Pneumonia and Macrophage Activation Syndrome-Like Disease. Autoimmunity Reviews 19, 102537 (2020). [PubMed: 32251717]
48. Veras FP, et al. SARS-CoV-2–triggered neutrophil extracellular traps mediate COVID-19 pathologySARS-CoV-2 directly triggers ACE-dependent NETs. Journal of Experimental Medicine 217(2020).
49. Wigerblad G & Kaplan MJ Neutrophil extracellular traps in systemic autoimmune and autoinflammatory diseases. Nature Reviews Immunology (2022).
50. Tanaka T, Narazaki M & Kishimoto T IL-6 in Inflammation, Immunity, and Disease. Cold Spring Harbor Perspectives in Biology 6(2014).

Methods REFERENCES

1. Rendeiro AF, et al. Profiling of immune dysfunction in COVID-19 patients allows early prediction of disease progression. Life Science Alliance 4, e202000955 (2021). [PubMed: 33361110]
2. Doron I., et al. Mycobiota-induced IgA antibodies regulate fungal commensalism in the gut and are dysregulated in Crohn's disease. Nature Microbiology 6, 1493–1504 (2021).
3. Beigel JH, et al. Remdesivir for the Treatment of Covid-19 — Final Report. New England Journal of Medicine 383, 1813–1826 (2020). [PubMed: 32445440]
4. Cheong J-G, et al. Epigenetic memory of coronavirus infection in innate immune cells and their progenitors. Cell 186, 3882–3902.e3824 (2023). [PubMed: 37597510]
5. Leonardi I., et al. $CX3CR1^{+}$ mononuclear phagocytes control immunity to intestinal fungi. Science 359, 232–236 (2018). [PubMed: 29326275]
6. Li X., et al. Response to Fungal Dysbiosis by Gut-Resident $CX3CR1^{+}$ Mononuclear Phagocytes Aggravates Allergic Airway Disease. Cell Host & Microbe 24, 847–856.e844 (2018). [PubMed: 30503509]
7. Yeung ST, Ovando LJ, Russo AJ, Rathinam VA & Khanna KM CD169+ macrophage intrinsic IL-10 production regulates immune homeostasis during sepsis. Cell Reports 42(2023).
8. Ural BB, et al. Identification of a nerve-associated, lung-resident interstitial macrophage subset with distinct localization and immunoregulatory properties. Science Immunology 5, eaax8756 (2020). [PubMed: 32220976]
9. Tang J, Iliev ID, Brown J, Underhill DM & Funari VA Mycobiome: Approaches to analysis of intestinal fungi. Journal of Immunological Methods 421, 112–121 (2015). [PubMed: 25891793]

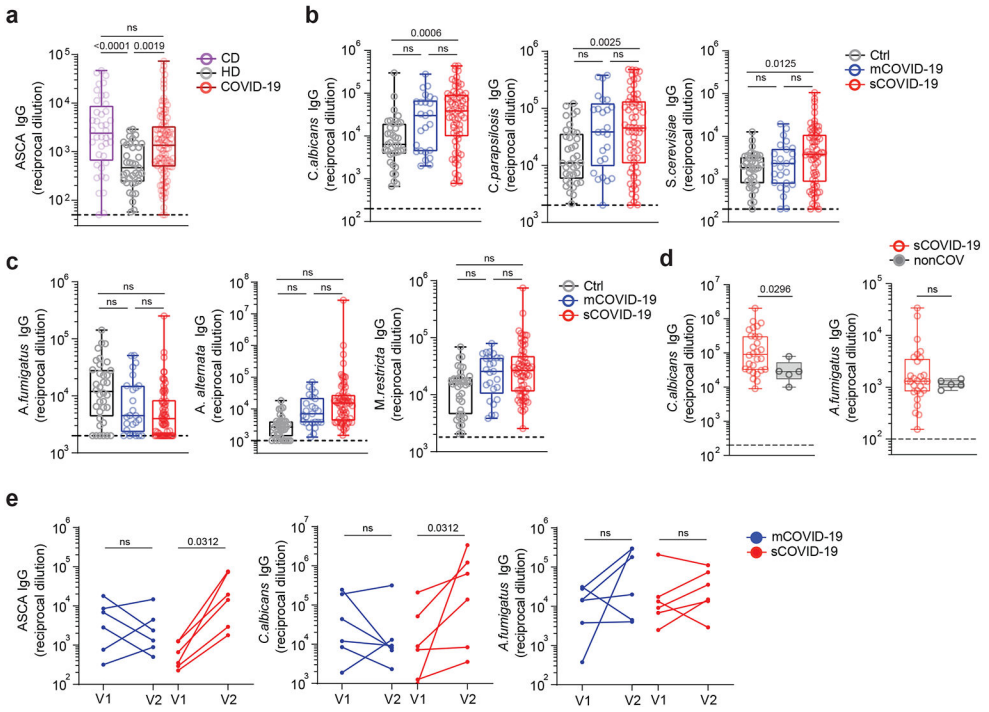

Figure 1. Antibodies to common intestinal fungi are elevated in COVID-19 patients.

a, Plasma antibody titers of circulating IgG to fungal mannan (*Saccharomyces cerevisiae*; ASCA) in Crohn's disease patients (CD, n=40), healthy individuals (HD, n=36) and COVID-19 patients (COVID-19, n=91). **b**, **c**, Plasma IgG antibody titers to *C. albicans* IgG (ACAL IgG), *C. parapsilosis* IgG and *S. cerevisiae* IgG (**b**) or *A. fumigatus* IgG, *A. alternata* IgG and *M. restricta* IgG (**c**) in HD (n=36), mCOVID-19 (n=25) and sCOVID-19 (n=66) (Supplementary Table 1). Mild and moderate patients were grouped together as mCOVID-19 for analysis against sCOVID-19 or HD. **d**, Plasma IgG antibody titers to *C. albicans* and *A. fumigatus* IgG in sCOVID-19 (n=28) and non-COVID-19 patients admitted in the intensive care unit (nonCOV, n=5) (Supplementary Table. 2). **e**. Longitudinal assessment of plasma IgG antibody titers to ASCA, *C. albicans* (ACAL) and *A. fumigatus* IgG in mCOVID-19 (n=6) and sCOVID-19 (n=6). Samples are collected at clinical diagnosis of infection or first administration (V1) and during the development of acute disease stage (V2; more than two weeks post-V1). All data are shown as endpoint titers normalized to ELISA reciprocal dilution. The dotted line indicates the limit of detection. For all boxplots, the center is drawn through the median of the measurement, and the lower and upper bounds of the box correspond to the first and third quartile. The whiskers go down to the smallest value and up to the largest. Statistical significance was determined by the one-way ANOVA followed by Tukey's multiple-comparison in **a-c**, a two-tailed Mann-Whitney test in **d**, and a two-tailed Wilcoxon matched-pairs singled-rank test in **e**. ns=not significant.

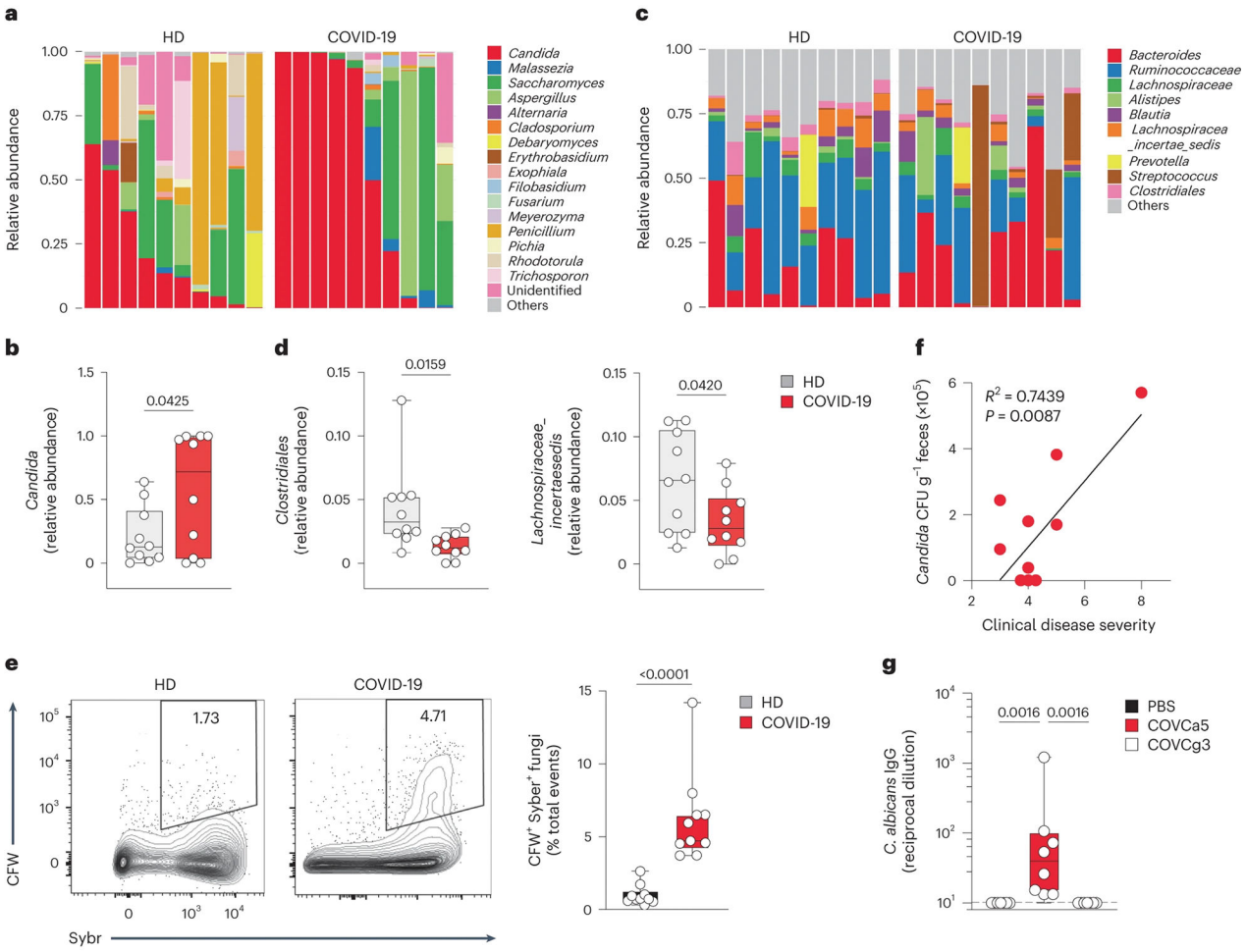

Figure 2. *Candida* species of the gut mycobiota expand in sCOVID-19.

a, **b**, Stack plot of relative abundances at the genus level for the 17 fungal genera with the highest average abundance (**a**) or the 9 bacterial genera with the highest average abundance (**b**) assessed by ITS1 sequencing of fungal rDNA or 16S sequencing of bacterial rDNA from stool samples of HD (n=10) and sCOVID-19 (n=10) in cohort 3 (Supplementary Table 3 and 4). **c**,**d**, Relative abundance of *Candida* (**c**) or *Clostridiales* and *Lachnospiraceae* (**d**) as in a. Lower and upper hinges correspond to the first and third quartile. **e**, Linear regression analysis of *Candida* species (CFU/g of stool) in COVID-19 patient stool (n=10) and disease severity as defined by an eight-category ordinal scale score (see Methods). **f**, Representative flow cytometry plots for Multi-KAP-based assessment of fungal biomass (CFW^+ Sybr $Green^+$) and the percentage of CFW^+ Sybr $Green^+$ cells per total event from fecal samples of COVID-19 (n=10) and HD (n=10) in cohort 3 (Supplementary Table 3 and 4). Insets indicate percentage of cells within the gate in representative plots. **g**, *C. albicans* specific IgG titers in the serum of antibiotic-treated mice two weeks after oral gavage with either PBS (n = 7), *C. albicans* (COVCa5, n = 8) or *C. glabrata* (COVCa3, n = 7) strains isolated from COVID-19 patient's stool. The results were pooled from two experiments. For all boxplots, the center is drawn through the median of the measurement, and the lower and upper bounds of the box correspond to the first and third quartile. The whiskers go down to

the smallest value and up to the largest. Plots represent individual patients (**b**, **d, e, f**) and mice (**g**). P values were calculated using a two-tailed Mann-Whitney test in **b, d** and **f** and the one-way ANOVA followed by Tukey's multiple-comparison in **g.** ns=not significant.

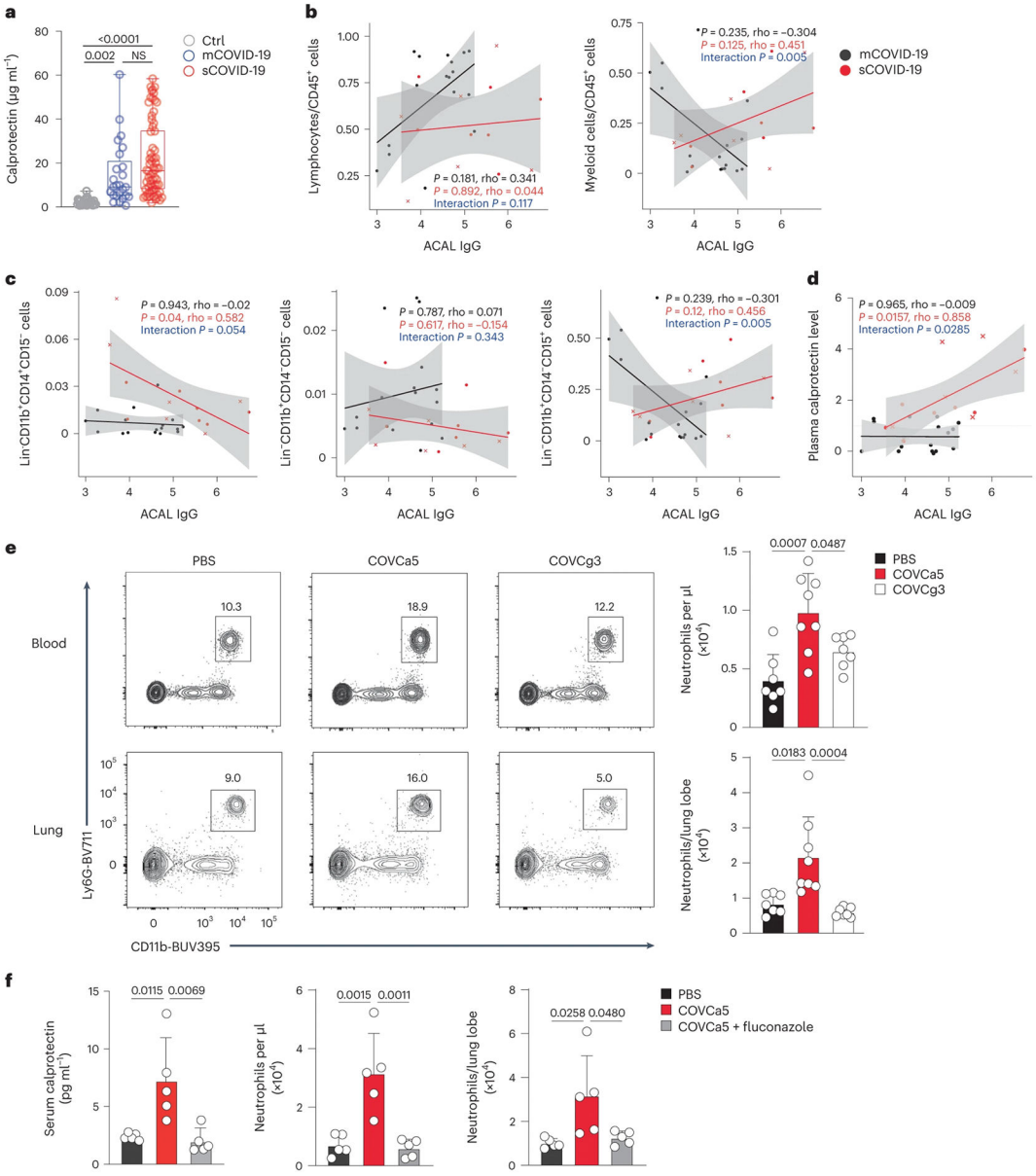

Figure 3. Neutrophils and ACAL IgG differentiate mCOVID-19 from sCOVID-19, and link intestinal *Candida* overgrowth to proinflammatory immunity in the lung.

a, Calprotectin plasma levels in HD (n=36), mCOVID-19 (n=25) and sCOVID-19 (n=66) from cohort 1 (Supplementary Table 1). **b-d**, Scatter plots of lymphocytes and myeloid cells (**b**) and $Lin^{-}CD11b^{+}CD14^{+}CD15^{-}$ monocytes (MO), $Lin^{-}CD11b^{+}CD14^{-}CD15^{-}$ monocyte-derived cells (MC) and $Lin^{-}CD11b^{+}CD14^{-}CD15^{+}$ polymononuclear neutrophils/granulocytes (PMNs) frequencies (**c**) in the blood (b,c) and calprotectin levels in the plasma (**d**) against levels of ACAL plasma IgG in sCOVID (n=13) and mCOVID-19 (n=17) from cohort 1(Supplementary Table 1). Crosses indicate deceased patients. Red and black lines show linear fits within severe and low to moderate groups, respectively, with 95% confidence intervals shown in gray. Spearman correlation estimates (rho) and associated p values are shown in red and black for sCOVID-19 and mCOVID-19, respectively. **e.**

Representative plots and the number of $CD45^+Ly6G^+CD11b^+$ neutrophils in peripheral blood and lung at week 2 after intestinal colonization of antibiotic-treated mice with either *C. albicans* (COVCa5, n=8) or *C. glabrata* (COVCa3, n=7), or oral gavage with PBS (n = 7). Insets indicate the percentage of cells within the gate. The results were pooled from two experiments. **f**, Serum calprotectin and the number of $Ly6G^+CD11b^+$ neutrophils in peripheral blood and lung at week 2 in mice that received oral gavage with PBS (n=5), COVCa5 (n=5) or COVCa5 followed by treatment with fluconazole two days after COVCa5 colonization (COVCa5 + fluconazole, n=5). Data in **f** are representative of two experiments. For boxplots in **a**, the center is drawn through the median of the measurement, and the lower and upper bounds of the box correspond to the first and third quartile. The whiskers go down to the smallest value and up to the largest. The bar graphs presented as mean ± SEM. Plots represent individual patients (**a-d**) and mice (**e, f**). Correlation analysis in b-d were assessed using the Spearman correlation coefficient with a two-tailed test. Differing correlations between severe versus mild/moderate groups were assessed by evaluating the significance of an interaction. P values were calculated using the one-way ANOVA followed by Tukey's multiple-comparison in a and Kruskal–Wallis test with a Dunn’s posttest in e and f. ns=not significant.

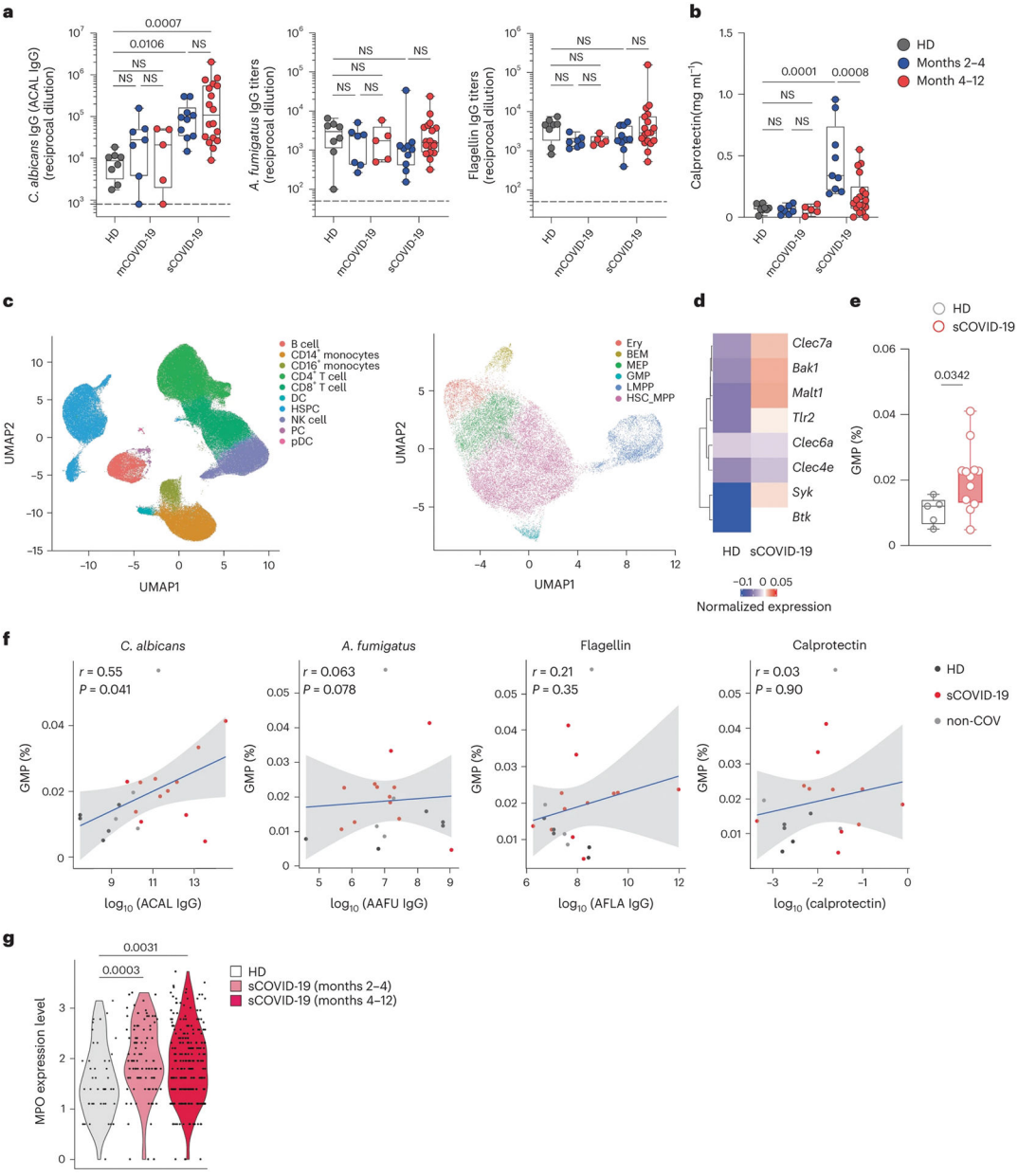

Figure 4. Persistently altered function of neutrophil progenitors in patients recovering from sCOVID-19.

a, b, Plasma IgG antibody titers to *C. albicans* (ACAL IgG), *A. fumigatus* and flagellin (**a**) or calprotectin levels (**b**) in HD (n=8) and patients recovering from mCOVID-19 month 2-4 (n=7), mCOVID-19 month 4-12 (n=5), sCOVID-19 month 2-4 (n=10) and sCOVID-19 month 4-12 (n=18) (Supplementary Table 2). **c**, Subject-paired analysis of PBMCs (left) and HSPC subsets (right) with enrichment of $CD34^+$ HSPC from PBMC followed by combined single-nuclei RNA/ATAC-seq (Multiome). Plots in HSPC were annotated for major progenitor cell types; erythroid progenitor cells (Ery), basophil-eosinophil-mast cell progenitor cells (BEM), lymphoid-primed multipotent progenitor cells (LMPP), megakaryocyte-erythroid progenitor cells (MEP), hematopoietic stem cells/

multipotent progenitor cells (HSC/MPP), granulocyte-macrophage progenitor cells (GMP). **d,** Heatmap representation of differentially expressed genes involved in antifungal immunity and signaling by HSPC from HD (n=5) and sCOVID-19 (n=12). **e,** Boxplots representing the frequency of GMPs in enriched $CD34^+$ HSPC from HD (n=5) and sCOVID-19 (n=12). The data in **e** and **f** represents normalized expression by sctranform[34]. **f**, Correlation and linear regression of anti-fungal (*C. albicans* or *A. fumigatus*) or anti-bacterial (flagellin) IgG antibodies (log10 titer) or calprotectin levels (log10 concentration) with frequency of GMP. Each dot represents HD (5), sCOVID (n=12) and nonCOV (n=5). Blue line indicates the regression line for all patients. The associated linear regression equation, Pearson's correlation. Coefficient, and significance are shown. **g**, Violin plots showing distribution of MPO expression in GMPs at month 2-4 (n=4) and month 4-12 (n=8) post hospital admission of sCOVID-19 versus HD (n=5). For boxplots in **a, b** and **e**, the center is drawn through the median of the measurement, and the lower and upper bounds of the box correspond to the first and third quartile. The whiskers go down to the smallest value and up to the largest. Dots represent individual patients (**a, b, e, f**) and cells (**g**). P values were calculated using the one-way ANOVA followed by Tukey's multiple-comparison in a, b and a two-tailed Mann-Whitney test in e and Kruskal–Wallis test with a Dunn's posttest in g. ns=not significant.

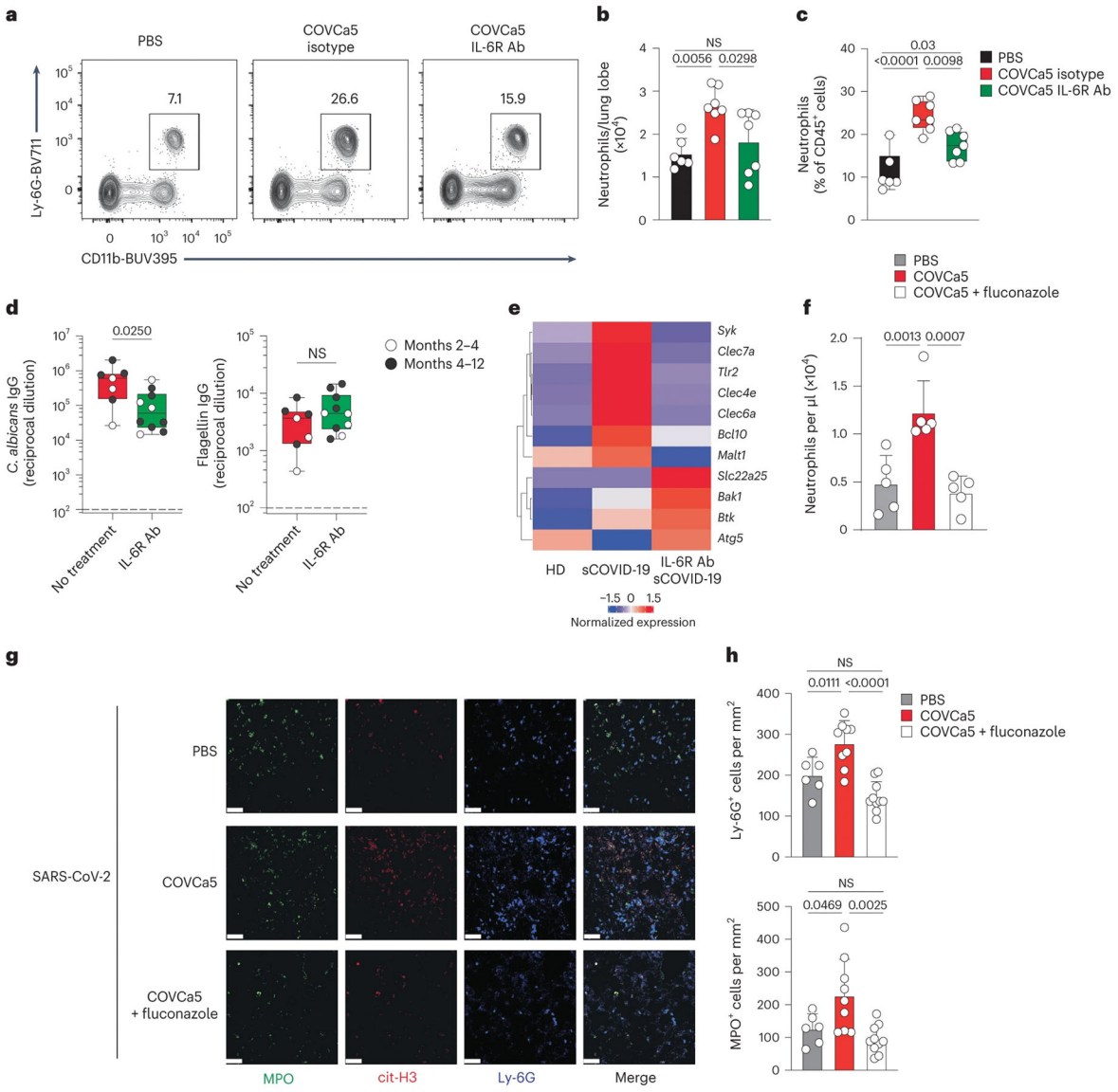

Figure 5. IL-6 mediates immune activation in severe COVID-19 patients and in a mouse model of COVID-19 during *C. albicans*-aggravated lung NETosis.

a, Representative dot plots of lung $CD45^+CD11b^+Ly\text{-}6G^+$ neutrophils from COVCa5-colonized mice treated with IL-6R (n=7) or isotype (n=7) antibodies every other day for two weeks post-colonization or were left uncolonized and untreated (PBS, n=6). Insets indicate percentage of cells within the gate. **b**, Absolute numbers and **c,** percentage of $CD45^+CD11b^+Ly\text{-}6G^+$ neutrophils in lung $CD45^+$ cells, as in **a**. **d**, Plasma IgG antibody titers to *C. albicans* and flagellin in sCOVID-19 month 2-4 and sCOVID-19 month 4-12 patients who received IL-6R blockade treatment during acute infection (IL-6R Ab, n=10) or not (no treatment, n=7). The results were pooled from two experiments. **e**, Heatmap of genes involved in fungal recognition in blood GMPs isolated from sCOVID-19 who received IL-6R blockade treatment (IL-6R Ab sCOVID, n=6) or not (sCOVID, n=7) during acute COVID-19 infection or from HD (n=7). **f-h,** Number of $Ly6G^+CD11b^+$ cells in the peripheral blood as assessed by flow cytometry (**f**) and immunofluorescence images (**g**) and

quantification (**h**) of $H3Cit^+$, MPO^+ and Ly-$6G^+$ neutrophils from multiple fields (20×) of lung sections (g) at day 5 post intranasal inoculation with SARS-COV-2 in mice that were uncolonized (PBS, n=5) or colonized with COVCa5 at day -14 before infection (Extended Data Figure 6b) and left untreated (n=5) or treated with fluconazole (n=5) two days after colonization for the duration of the experiment. White scale bar (g) indicates 30 μm. Image analysis was conducted on acquired images as follows: two slides per animal of n = 3-5 animals. The data are representative of two experiments. For boxplots in c,d, the center is drawn through the median of the measurement, and the lower and upper bounds of the box correspond to the first and third quartile. The whiskers go down to the smallest value and up to the largest. The bar graphs in b, f and h presented as mean ± SEM. Dots represent individual patients (**d**) and mice (**b, c, f, h**). P values were calculated using the one-way ANOVA followed by Tukey's multiple-comparison in b, c, f and h and a two-tailed Mann-Whitney test in d. ns=not significant.